NASA TM X-294

TECHNICAL MEMORANDUM
X-294

ANALYTICAL INVESTIGATION AND PREDICTION OF SPIN AND RECOVERY CHARACTERISTICS OF THE NORTH AMERICAN X-15 AIRPLANE

By William D. Grantham and Stanley H. Scher

Langley Research Center
Langley Field, Va.

Declassified October 25, 1962

NATIONAL AERONAUTICS AND SPACE ADMINISTRATION
WASHINGTON

October 1960

NATIONAL AERONAUTICS AND SPACE ADMINISTRATION

TECHNICAL MEMORANDUM X-294

ANALYTICAL INVESTIGATION AND PREDICTION OF SPIN AND RECOVERY CHARACTERISTICS OF THE NORTH AMERICAN X-15 AIRPLANE

By William D. Grantham and Stanley H. Scher

SUMMARY

An analytical study has been made to aid in predicting the spin and recovery characteristics of the North American X-15 atmospheric-reentry research airplane. The approach used was to simulate first on a high-speed digital computer the spin entry, the ensuing spin, and the recovery therefrom obtained from dynamic-model tests at low Reynolds number by using appropriate aerodynamic force and moment data. Then, high Reynolds number aerodynamic data were inserted into the computer and the resulting effects on spin entry and spin characteristics were calculated.

The results indicated that the airplane with the lower rudder on or off is not likely to enter a spin from trimmed gliding or level flight. A developed spin might be obtained if the airplane receives some violent disturbance which would tend to put it in a flight condition having rotation and a high angle of attack, approximating the attitude and motion of a model when launched into a spin tunnel. Such a spin would probably be more readily obtainable when the lower rudder is off than when it is on, and the ensuing spin would be flatter and faster. Recovery from the initial phase of this motion would be satisfactory for either configuration. However, if the spin is allowed to develop fully, difficulty may be experienced in effecting a recovery for the lower-rudder-off configuration, but for the lower-rudder-on configuration satisfactory recovery would be obtainable by optimum control technique.

The results of the investigation also indicated that the magnitude of the static pitching moment, the effective dihedral, and the pitch damping can be critical in the spin entry and spinning motions for modern aircraft similar to the subject configuration and may mean the difference between the airplane experiencing a spin or no spin.

INTRODUCTION

For a number of years, the Langley 20-foot free-spinning tunnel has been used to test small-scale dynamically ballasted models of airplanes. Properly interpreted, the results obtained from tests have usually been adequate for predicting the spin and recovery characteristics of airplanes represented by the dynamic models. However, modern trends in airplane design, primarily very long fuselage forebodies and mass distributed very heavily in the fuselage, have caused Reynolds number and spin-entry-technique differences between airplanes and models to become extremely important factors which sometimes have made proper interpretation of the spin-tunnel-model results quite difficult (ref. 1). Predicting the airplane spin and recovery behavior remains a serious problem, because modern high-speed airplanes in the categories of fighter, interceptor, and research airplanes continue to enter spins inadvertently with occasional loss of life and property.

L 9 5 3

In an attempt to enable better prediction of full-scale spin and recovery characteristics of modern design and to add to the general knowledge of how various design and control-sequence factors may affect spins and related post-stall transient motions, including incipient spins, two additional research and evaluation techniques have been initiated at the Langley Research Center to complement the free-spinning-tunnel tests. The two new techniques are the use of large radio-controlled free-flight dynamic models dropped at altitude and flown into various maneuvers conducive of spin entry (ref. 2), and the use of analytical techniques which enable calculations of the motions to be made on a high-speed automatic digital computer by using static and rotary wind-tunnel aerodynamic data and six-degree-of-freedom equations of motion (refs. 1 and 3).

As regards the analytical technique using a digital computer, independent investigations described in references 3 and 4 for current delta-wing and sweptback-wing fighter airplanes, respectively, have indicated that it is possible to simulate known airplane spin-entry, developed-spin, and recovery motions provided adequate aerodynamic-data coefficients from measurements or estimations are used. Developed to its ultimate, the analytical technique should enable the prediction of an airplane's spin and recovery characteristics before full-scale flights are made. The accuracy of such a prediction will, of course, depend on how accurately the required aerodynamic data have been obtained in wind tunnels or by estimations and how representative are these data of the full-scale airplane.

The analytical study described in this paper was made to aid in the prediction of the spin and recovery characteristics of the North American X-15 airplane and was conducted in conjunction with free-spinning-tunnel

tests made on a 1/30-scale dynamic model (unpublished results) and with tests on a 1/7-scale radio-controlled model dropped from a helicopter (ref. 5). The experimental tests of these X-15 models were made at relatively low Reynolds numbers, and it was believed that Reynolds number effects on the fuselage forebody might appreciably alter the spin and recovery characteristics of this design.

The approach used in the analytical study was to use low Reynolds number aerodynamic force and moment data first to try to simulate the spin entry, the ensuing spin, and the recovery therefrom obtained from dynamic-model tests. Then, high Reynolds number data from reference 6 were inserted into the computer and the resulting effects on spin entry and spin characteristics were calculated.

SYMBOLS

The body system of axes is used. This system of axes, related angles, and positive directions of corresponding forces and moments are illustrated in figure 1.

b wing span, ft

C_l rolling-moment coefficient, $\dfrac{M_X}{\frac{1}{2}\rho V_R^2 Sb}$

C_m pitching-moment coefficient, $\dfrac{M_Y}{\frac{1}{2}\rho V_R^2 S\bar{c}}$

C_n yawing-moment coefficient, $\dfrac{M_Z}{\frac{1}{2}\rho V_R^2 Sb}$

C_X longitudinal-force coefficient, $\dfrac{F_X}{\frac{1}{2}\rho V_R^2 S}$

C_Y side-force coefficient, $\dfrac{F_Y}{\frac{1}{2}\rho V_R^2 S}$

C_Z	normal-force coefficient, $\frac{F_Z}{\frac{1}{2}\rho V_R^2 S}$
$\bar{c}$	mean aerodynamic chord, ft
F_X	longitudinal force acting along X body axis, lb
F_Y	lateral force acting along Y body axis, lb
F_Z	normal force acting along Z body axis, lb
g	acceleration due to gravity, 32.17 ft/sec^2
h_1	altitude at beginning of time increment, ft
h_2	altitude at end of time increment, ft
I_X, I_Y, I_Z	moments of inertia about X, Y, and Z body axes, respectively, slug-ft^2
l	maximum depth of fuselage where wing-fuselage intersect, ft
M_X	rolling moment acting about X body axis, ft-lb
M_Y	pitching moment acting about Y body axis, ft-lb
M_Z	yawing moment acting about Z body axis, ft-lb
m	mass of airplane, W/g, slugs
p,q,r	components of resultant angular velocity Ω about X, Y, and Z body axes, respectively, radians/sec
R	Reynolds number, Vl/ν
S	wing area, sq ft
t	time, sec
u,v,w	components of resultant velocity V_R along X, Y, and Z body axes, respectively, ft/sec
V	vertical component of velocity of airplane center of gravity (rate of descent), ft/sec

V_R	resultant linear velocity, ft/sec
W	weight, lb
X,Y,Z	body axes
α	angle of attack, angle between relative wind V_R projected into XZ-plane of symmetry and X body axis, positive when relative wind comes from below XY body plane, deg
β	angle of sideslip, angle between relative wind V_R and projection of relative wind on XZ-plane, positive when relative wind comes from right of plane of symmetry, deg
δ_a	aileron deflection (differential deflection of horizontal control) with respect to chord line of wing, positive with trailing edge of right aileron down, deg
δ_h	horizontal-tail deflection with respect to fuselage reference line, positive with trailing edge down, deg
δ_r	rudder deflection with respect to fin, positive with trailing edge to left, deg
θ_e	total angular movement of X body axis from horizontal plane measured in vertical plane, positive when airplane nose is above horizontal plane, radians or deg
ν	kinematic viscosity, ft^2/sec
ρ	air density, slugs/cu ft
ϕ	angle between Y body axis and horizontal measured in vertical plane, positive for erect spins when right wing downward and for inverted spins when left wing downward, deg
ϕ_e	total angular movement of Y body axis from horizontal plane measured in YZ body plane, positive when clockwise as viewed from rear of airplane (if X body axis is vertical, ϕ_e is measured from a reference position in horizontal plane), radians
ψ_e	horizontal component of total angular deflection of X body axis from reference position in horizontal plane, positive when clockwise as viewed from vertically above airplane, radians

Ω resultant angular velocity, radians/sec (or rps where noted)

$$C_{l_p} = \frac{\partial C_l}{\partial\left(\frac{pb}{2V_R}\right)}$$

$$C_{m_q} = \frac{\partial C_m}{\partial\left(\frac{q\bar{c}}{2V_R}\right)}$$

$$C_{n_r} = \frac{\partial C_n}{\partial\left(\frac{rb}{2V_R}\right)}$$

$$C_{l_{\dot{\beta}}} = \frac{\partial C_l}{\partial\left(\frac{\dot{\beta}b}{2V_R}\right)}$$

$$C_{m_{\dot{\alpha}}} = \frac{\partial C_m}{\partial\left(\frac{\dot{\alpha}\bar{c}}{2V_R}\right)}$$

$$C_{n_{\dot{\beta}}} = \frac{\partial C_n}{\partial\left(\frac{\dot{\beta}b}{2V_R}\right)}$$

$$C_{l_\beta} = \frac{\partial C_l}{\partial \beta}$$

$$C_{n_\beta} = \frac{\partial C_n}{\partial \beta}$$

$$C_{Y_\beta} = \frac{\partial C_Y}{\partial \beta}$$

$\Delta C_{l,a}$ incremental rolling-moment coefficient due to aileron deflection

$\Delta C_{l,r}$ incremental rolling-moment coefficient due to rudder deflection

$\Delta C_{n,a}$ incremental yawing-moment coefficient due to aileron deflection

$\Delta C_{n,r}$ incremental yawing-moment coefficient due to rudder deflection

$\Delta C_{Y,a}$ incremental side-force coefficient due to aileron deflection

$\Delta C_{Y,r}$ incremental side-force coefficient due to rudder deflection

A dot over a symbol represents a derivative with respect to time; for example, $\dot{u} = \frac{du}{dt}$.

PROCEDURES AND CALCULATIONS

Spin entry and spin motions were calculated by a high-speed digital computer which solved the equations of motion and associated formulas listed in the appendix. The equations of motion are Euler's equations representing six degrees of freedom along and about the airplane body system of axes. (See fig. 1 for illustration of body axes.) The mass and dimensional characteristics used in the calculations are listed in table I and a three-view sketch of the airplane is shown in figure 2.

Most of the aerodynamic data used were nonlinear and are presented in the plots shown in figures 3 to 12. The data in figures 3 to 7 were based on measurements obtained in the Langley free-flight tunnel for a Reynolds number of about 430,000 based on $\bar{c}$ and of about 195,000 based on the maximum vertical depth of the model fuselage nose section. The data in figures 8 to 10 were obtained in the Langley high-speed 7- by 10-foot tunnel for a Reynolds number of about 2,000,000 based on $\bar{c}$ and of about 865,000 based on the maximum vertical depth of the model fuselage nose section. Values of the damping-in-pitch derivative C_{m_q} were held constant $\left(C_{m_q} = -10.0\right.$ as obtained from low-angle-of-attack tests in ref. 7$\left.\right)$ for most of the investigation. However, during the investigation measured values for the range of α between the stall and 90° were obtained in a separate wind-tunnel investigation and were used in some

of the final calculations of this investigation. These measured values of C_{m_q} are shown in figure 12.

The rotary derivatives presented in figures 7 and 12 were obtained as combination derivatives which include the effects of $\dot{\beta}$ and $\dot{\alpha}$ - that is, C_{l_p} is actually $\left(C_{l_p} + C_{l_{\dot{\beta}}} \sin \alpha\right)$, C_{n_r} is actually $\left(C_{n_r} - C_{n_{\dot{\beta}}} \cos \alpha\right)$ and C_{m_q} is actually $\left(C_{m_q} + C_{m_{\dot{\alpha}}}\right)$. However, inasmuch as the full derivatives could not be separated into their component parts, it was arbitrarily decided for this investigation to treat the derivatives as though they were due solely to angular velocities about body axes. These damping derivatives, as well as the incremental force and moment coefficients due to deflection of the ailerons and rudder, were available only from low Reynolds number tests and were arbitrarily assumed to be invariant with Reynolds number.

L 9 5 3

For the calculations made in an attempt to simulate spin entries like that of the radio-controlled model or of an airplane, the effect of the variation of air density with altitude was included. For the type of calculation simulating conditions under which the model is launched into a spin tunnel, air density was maintained constant as it is in the Langley 20-foot free-spinning tunnel, and representative initial values of attitude and rate of rotation were selected. The inputs simulating airplane control movements were introduced into the computer by means of appropriate switches. The timing and direction of these inputs were based on observed time histories of the computed motion as presented by computer print-out tables.

The significance of motions calculated after application of controls for attempted recoveries was evaluated on the basis of the following considerations: An airplane is considered to have recovered from a spin when the angle of attack at the center of gravity has gone below the angle of attack at which the wing stalls. Usually, when this attitude is achieved, the airplane enters a steep dive without rotation ($r = 0$). In some cases, however, the airplane may be turning or rolling in a spiral glide or an aileron roll. Also, sometimes, the airplane may roll or pitch to an inverted attitude from the erect spin and may still have some rotation but is out of the original erect spin.

For convenience, a list of the aerodynamic data used in this investigation is presented in table II.

BRIEF REVIEW OF DYNAMIC-MODEL-TEST RESULTS

Results reported in reference 5 and represented for convenience in figure 13 indicate that the 1/7-scale dynamic radio-controlled model with lower rudder off and its center of gravity at 19.5 percent $\bar{c}$ was flown into a spin-entry maneuver from trimmed gliding flight and, with the differentially operable horizontal tail maintained in an aileron-against-the-spin position (stick left in a spin to the pilot's right), made a three-turn spin during which the angle of attack varied from 60° to 90° and in which the rate of spin rotation averaged about 1.1 radians per second (0.175 rps) for the three turns. Good spin recovery was achieved from that spin by reversing the differential tails, hereinafter referred to as ailerons, to with the spin, as is also shown in figure 13. Results of free-spinning tunnel tests made at the Langley Research Center with a 1/30-scale dynamic model with lower rudder off and ailerons against the spin indicated that, for center-of-gravity positions ranging from 0 percent to 20 percent $\bar{c}$, fully developed spins were possible in which Ω could be as high as 1.85 radians per second (0.335 rps) and in which α varied from about 60° to 90°. From these spins, recoveries varied from fast to slow and, on this basis, recovery characteristics were considered unsatisfactory (lower rudder off).

L 9 5 3

RESULTS AND DISCUSSION

Calculated results of the analytical study are presented in figures 14 to 26 as time histories of angle of attack α, angle of wing tilt ϕ, yawing velocity r or resultant angular velocity Ω, control-surface positions, and spinning turns completed. Although only these few pertinent variables of the motions are presented, time histories of all the attitude, velocity, and acceleration variables in the equations of motion were obtained.

Low Reynolds Number Calculations With Lower Rudder Off

Calculations were made to simulate the result (fig. 13) which was obtained during a flight of the 1/7-scale radio-controlled model at low Reynolds number and with the lower rudder off. Zero-time conditions for the calculations were estimated from the results of the model test and are listed in column A of table III. The initial calculated results, shown in figure 14, did not agree with the model results (fig. 13), but rather indicated a continuing cyclic motion in pitch with variations of angle of attack between 20° and 80° and with a rate of rotation averaging about 0.7 radian per second. Because of the large oscillations in pitch, it was reasoned that perhaps some adjustment was desirable to the

magnitudes of aerodynamic pitching moments used. From an examination of some pitching-moment data plotted against sideslip angle for this configuration (ref. 5), it was apparent that large reductions in negative values of C_m could occur when large sideslip angles are present, such as those obtained at high angles of attack during the calculated attempted spin entry. Considering this fact and also the assumption that shielding of the horizontal tail by the vertical stub and fuselage area under the horizontal tail would possibly reduce the aerodynamic nose-down pitching moment in a spinning motion, it was decided to investigate the effect of reducing the curve of C_m against α as an input into the equations of motion. Arbitrarily, the static-pitching-moment values (fig. 3) were reduced by approximately 50 percent and another calculation was made. The results are shown in figure 15, and after three turns of this calculated spin motion the angle of attack and rate of rotation agreed with those for the three-turn spin obtained during the model tests (fig. 13). A recovery from this spin (fig. 15) was attempted by reversing the ailerons and rudder, and recovery was obtained in approximately one turn, a result which also is in qualitative agreement with the experimental result.

It may be noted that included among the initial conditions for the spin-entry calculation just discussed (initial conditions are given in col. A of table III) was a nose-down attitude, $\theta_e = -60^\circ$, used to simulate the experimental model initial attitude. As a matter of interest, a calculation was made in which an attempt to enter a spin was started from an arbitrary nose-up attitude, $\theta_e = 20^\circ$. (See table III, col. B.) The results are shown in figure 16 and indicate a spin that for the first three turns was also generally similar to the experimentally obtained spin, as had been the three-turn spin calculated starting from the initial nose-low attitude. The results from both these calculated three-turn spins are considered to have simulated the experimental 1/7-scale-model spin adequately.

As may be seen in figure 16, no recovery was attempted from the second of the two calculated three-turn spins. Instead, pro-spin controls were maintained and, as can be seen, the spin-rotation rate continued to increase until after a total of eight spinning turns. At that time, Ω was averaging about 2.1 radians per second (0.335 rps). Perhaps if it had been practicable to allow the experimental model to spin longer, it too may have eventually increased its rate of rotation. At any rate, inasmuch as the 1/30-scale free-spinning-tunnel model had exhibited developed spins rotating as high as 1.85 radians per second (0.295 rps), as noted earlier, the calculated and experimental (spin tunnel) developed spins are considered to be in qualitative agreement, even though the calculated value of Ω was somewhat higher than the experimentally obtained value of Ω. As regards recovery characteristics from the developed spin, a recovery attempt by reversing ailerons

and rudder was made from the calculated spin after eight turns (fig. 16) and the result indicated no recovery in four turns. This is considered to be in qualitative agreement with the free-spinning-tunnel experimental result, which (as noted before) indicated unsatisfactory recovery characteristics with lower rudder off because recoveries varied from fast to slow.

High Reynolds Number Calculations

Inasmuch as it appeared at this point in the analytical study that the experimental model motions had been reasonably simulated, the low Reynolds number aerodynamic data were removed from the computer and corresponding high Reynolds number inputs were inserted for the attempts to calculate possible airplane spin characteristics. The aerodynamic data that were changed because of Reynolds number differences appear in figures 8 and 9 as plots of C_m, C_Z, C_X, C_{Y_β}, C_{n_β}, and C_{l_β} against α. As mentioned previously, the damping derivatives and the incremental force and moment coefficients due to deflection of ailerons and rudder, all measured only at low Reynolds number, were not changed for the high Reynolds number calculations. Also, because the aerodynamic-data measurements indicated no significant difference in the damping coefficients between the lower-rudder-on and lower-rudder-off configurations in the high angle-of-attack range, the values used in the calculations for these damping coefficients are the same for lower rudder on and for lower rudder off. Incremental effects of the lower rudder on the static derivatives C_{n_β} and C_{l_β}, as well as on the incremental moments due to rudder deflection, were appreciable, however, and these effects were included in the calculation inputs.

Lower rudder on, simulated launching with rotary motion.- In order to determine whether the configuration with lower rudder on would spin at high Reynolds number, a launching with spin rotation was simulated. The initial conditions used for this launching were obtained from free-spinning-tunnel model tests (table III, col. C). The calculated motion obtained is presented in figure 17 and indicates increasing oscillations in both pitch and roll as the rate of spin rotation increased. The motion oscillated out of range of the computer's ability to continue the calculation and no developed spin was achieved. Inasmuch as it had been found in the low Reynolds number calculations that 100 percent of the static pitching moment probably does not act during spins, the curve of C_m against α (fig. 8) was reduced approximately 50 percent and another calculation was made. The resulting motion is in figure 18 and, as can be seen, a very steady spin is indicated. In order to see whether a lesser reduction in the measured static pitching moment would allow the attainment of a spin, other calculations were made when 85 percent

and 70 percent of the measured static values of C_m were used. These calculations showed that with C_m = 85 percent there was no spin obtained, whereas with C_m = 70 percent there was a spin. As shown in figure 19, where C_m values approximately equal to 70 percent of the measured static values were used, the rate of rotation is higher than that obtained with C_m values of 50 percent (fig. 18), and such a result can be expected if a spin can be maintained (ref. 1). Also, a recovery was attempted from this spin motion (fig. 19), and it can be seen that the airplane recovered in approximately $2\frac{1}{2}$ turns after antispin controls were deployed (rudder and ailerons reversed).

In view of the aforementioned results, it might be said that the full-scale airplane with the lower rudder on would spin if it was launched into a spin and if the pitching moment acting during spins was no more than about 70 percent of the measured static values shown in figure 8.

Lower rudder on, simulated spin-entry motion.- Inasmuch as a spin was obtained after a launching with rotation, as indicated for the high Reynolds number case when values equal to 70 percent of the measured static values of C_m were used, some attempts were made to obtain a spin from a more normal entry maneuver for the configuration with lower rudder on. For this calculation, the initial conditions shown in table III, column D, were used together with the same set of aerodynamic-data inputs as was utilized for the spin-launching calculation when $C_m \approx 70$ percent of the measured static values (fig. 19). The resulting motion is shown in figure 20 and indicated a diverging oscillation which ended in the airplane experiencing no spin as the angle of attack went below zero. Although not presented, a calculation was also made with $C_m \approx 50$ percent of the measured static values and the results obtained were similar to those obtained with C_m values of 70 percent.

In an attempt to understand better the results just discussed, another spin-entry calculation was made in which larger negative values of C_{l_β} were used. (See fig. 4 for values.) Seventy percent C_m values were also used. The results are shown in figure 21 and indicate that a spin was now obtained from entry. The angle of attack during this spin was approximately 50° and r was about 0.7 radian/second. From these results, it appears that the X-15 airplane with lower rudder on will not enter a spin from this type of entry because of the magnitude of the dihedral effect.

Lower rudder off, simulated launching with rotary motion.- In order to investigate the spin characteristics, at high Reynolds number, of the

lower-rudder-off configuration, a calculation was made in which the airplane was launched with applied spin rotation and with $C_m \approx 70$ percent of the measured static values. The result is shown in figure 22. A comparison of figures 22 and 19 indicates that the lower-rudder-off spin is flatter and faster than the lower-rudder-on spin, as would be expected. It can also be seen that the airplane did not recover from this fast-rotating spin (fig. 22), whereas it had recovered in $2\frac{1}{2}$ turns for the slower rotating spin shown in figure 19 for the lower-rudder-on case.

Lower rudder off, simulated spin-entry motion.- In an attempt to obtain a spin from a more normal type of entry for the lower-rudder-off configuration by using high Reynolds number data, the initial conditions shown in table III, column D, and C_m values 70 percent of the measured static values were used. The results indicated that the airplane experienced no spin in that the angle of attack went below zero. Another similar calculation was made with $C_m \approx 50$ percent of the measured static values and again no spin was indicated.

At this point a calculation was made to see what effect further reduction in the aerodynamic-pitching-moment input would have on the tendency to enter a spin. The C_m values shown in figure 11 were used and the results, shown in figure 23, indicate that a spin was attained. Although not investigated, it is believed that, if larger negative values of C_{l_β} along with C_m values equal to 70 percent of the measured static values had been used, as had been done for the lower-rudder-on calculations, they would have also enabled the attainment of a spin. In view of these considerations and some additional unpresented calculation results, indications are that the magnitudes of static pitching moment and effective dihedral have important interrelated effects as regards the determination of whether the subject configuration will spin. It appears that, when relatively large nose-down aerodynamic pitching moments are present, corresponding large amounts of effective dihedral are required for the attainment and maintenance of spins.

From the results just discussed, it appears that even the lower-rudder-off configuration at high Reynolds number will not enter a spin from gliding-flight attitudes. Factors contributing to the prevention of spins would be the magnitudes of the pitching and rolling moments present. However, if the airplane could, for some reason, achieve an attitude and motion simulating a rotary launching, such as is obtained in a free-spinning tunnel, the airplane could probably enter a spin.

Importance of Magnitude of Pitch Damping

As stated previously, a constant value of -10.0 (based on results in ref. 7) was used for C_{m_q} in most of the calculations. It was decided to investigate briefly the effects of varying C_{m_q} on the spin. The spin motion shown in figure 22 was arbitrarily chosen. With the same conditions used as inputs, but with $C_{m_q} = -5.0$, a calculation was made and the resulting motion is shown in figure 24. A comparison of figures 22 and 24 indicates that this reduction in C_{m_q} had little or no effect on the spinning motion when the airplane was launched with applied spin rotation.

In order to see whether a reduction in C_{m_q} would have any effect on a spin motion obtained from entry without applied rotation, calculations were made which had the same initial inputs as shown in figure 23 except for different values of C_{m_q}. The first arbitrary value used was $C_{m_q} = -7.0$. The results are shown in figure 25 and indicate that now a spin could not be attained. Because of the indicated importance of the magnitude of C_{m_q} as affecting spin entry, some wind-tunnel tests were made (as previously indicated) to determine the variation of C_{m_q} with angle of attack for this design. The measured results are shown in figure 12. A spin-entry calculation, without applied rotation, was made by using this curve as an input; the results are given in figure 26 and indicated that a spin motion was again attained and that this spin was similar to the one in which the constant $C_{m_q} = -10.0$ was used (fig. 23). It may be concluded from these results that the values of C_{m_q} used as an input can make a difference between the airplane experiencing a spin or no spin. Indications are that carefully measured values of this derivative for angles of attack ranging from 0° to 90° are desirable in analytical spin studies.

CONCLUDING REMARKS

The North American X-15 airplane with the lower rudder on or off is not likely to enter a spin from trimmed gliding flight. A developed spin might be obtained if the airplane receives some violent disturbance which would tend to put it in a flight condition having rotation and a high angle of attack, approximating the attitude and motion of the model when launched into a spin tunnel. Such a spin would probably be more readily

obtainable when the lower rudder is off than when it is on, and the ensuing spin would be flatter and faster. Recovery from the initial phase of this motion would be satisfactory for either configuration. However, if the spin is allowed to develop fully, difficulty may be experienced in effecting a recovery for the lower-rudder-off configuration, but for the lower-rudder-on configuration satisfactory recovery would be obtainable by optimum control technique.

The magnitude of static pitching moment, effective dihedral, and pitch damping can be critical in the spin entry and spinning motions for modern aircraft similar to the subject configuration and may mean the difference between the airplane experiencing a spin or no spin.

Langley Research Center,
National Aeronautics and Space Administration,
Langley Field, Va., March 16, 1960.

APPENDIX

EQUATIONS OF MOTION AND ASSOCIATED FORMULAS

The equations of motion used in calculating the spinning motions were:

$$\dot{p} = \frac{I_Y - I_Z}{I_X} qr + \frac{\rho V_R^2 Sb}{2I_X} C_{l_\beta}\beta + \frac{\rho V_R Sb^2}{4I_X} C_{l_p} p + \frac{\rho V_R^2 Sb}{2I_X} \Delta C_{l,r} + \frac{\rho V_R^2 Sb}{2I_X} \Delta C_{l,a}$$

$$\dot{q} = \frac{I_Z - I_X}{I_Y} pr + \frac{\rho V_R^2 S\bar{c}}{2I_Y} C_m + \frac{\rho V_R S\bar{c}^2}{4I_Y} C_{m_q}$$

$$\dot{r} = \frac{I_X - I_Y}{I_Z} pq + \frac{\rho V_R^2 Sb}{2I_Z} C_{n_\beta}\beta + \frac{\rho V_R Sb^2}{4I_Z} C_{n_r} r + \frac{\rho V_R^2 Sb}{2I_Z} \Delta C_{n,r} + \frac{\rho V_R^2 Sb}{2I_Z} \Delta C_{n,a}$$

$$\dot{u} = -g \sin \theta_e + vr - wq + \frac{\rho V_R^2 S}{2m} C_X$$

$$\dot{v} = g \cos \theta_e \sin \phi_e + wp - ur + \frac{\rho V_R^2 S}{2m} C_{Y_\beta}\beta + \frac{\rho V_R^2 S}{2m} \Delta C_{Y,r} + \frac{\rho V_R^2 S}{2m} \Delta C_{Y,a}$$

$$\dot{w} = g \cos \theta_e \cos \phi_e + uq - vp + \frac{\rho V_R^2 S}{2m} C_Z$$

In addition, the following formulas were used:

$$\alpha = \tan^{-1} \frac{w}{u}$$

$$\beta = \sin^{-1} \frac{v}{V_R}$$

$$V_R = \sqrt{u^2 + v^2 + w^2}$$

$$\Omega = \sqrt{p^2 + q^2 + r^2}$$

$$V = -u \sin \theta_e + v \cos \theta_e \sin \phi_e + w \cos \theta_e \cos \phi_e$$

$$h_2 = h_1 - \Delta t V$$

$$\dot{\theta}_e = q \cos \phi_e - r \sin \phi_e$$

$$\dot{\phi}_e = p + r \tan \theta_e \cos \phi_e + q \tan \theta_e \sin \phi_e$$

$$\dot{\psi}_e = \frac{\dot{\phi}_e - p}{\sin \theta_e}$$

$$\text{Turns in spin} = \frac{\int \dot{\psi}_e \, dt}{2\pi}$$

$$\phi_e = \sin^{-1} \frac{\sin \phi}{\cos \theta_e}$$

REFERENCES

1. Neihouse, Anshal I., Klinar, Walter J., and Scher, Stanley H.: Status of Spin Research for Recent Airplane Designs. NASA TR R-57, 1960. (Supersedes NACA RM L57F12.)

2. Libbey, Charles E., and Burk, Sanger M., Jr.: A Technique Utilizing Free-Flying Radio-Controlled Models To Study the Incipient- and Developed-Spin Characteristics of Airplanes. NASA MEMO 2-6-59L, 1959.

3. Scher, Stanley H., Anglin, Ernie L., and Lawrence, George F.: Analytical Investigation of Effect of Spin Entry Technique on Spin and Recovery Characteristics for a 60° Delta-Wing Airplane. NASA TN D-156, 1959.

4. Wykes, John H., Casteel, Gilbert R., and Collins, Richard A.: An Analytical Study of the Dynamics of Spinning Aircraft. Part I - Flight Test Data Analyses and Spin Calculations. WADC Tech. Rep. 58-381, Pt. I (ASTIA Doc. No. AD 203788), U.S. Air Force, Dec. 1958.

5. Hewes, Donald E., and Hassell, James L., Jr.: Subsonic Flight Tests of a 1/7-Scale Radio-Controlled Model of the North American X-15 Airplane With Particular Reference to High Angle-of-Attack Conditions. NASA TM X-283, 1960.

6. Bowman, James S., Jr., and Grantham, William D.: Low-Speed Aerodynamic Characteristics of a Model of a Hypersonic Research Airplane at Angles of Attack up to 90° for a Range of Reynolds Numbers. NASA TN D-403, 1960.

7. Lopez, Armando E., and Tinling, Bruce E.: The Static and Dynamic-Rotary Stability Derivatives at Subsonic Speeds of a Model of the X-15 Research Airplane. NACA RM A58F09, 1958.

TABLE I.- MASS AND DIMENSIONAL CHARACTERISTICS

[Values given in terms of full-scale airplane]

	Low Reynolds number calculations (same as 1/7-scale dynamic model)	High Reynolds number calculations (from airplane data)
$\bar{c}$, ft	10.27	10.27
b, ft	22.36	22.36
S, sq ft	200	200
W, lb	12,575	13,377
Center-of-gravity location, percent $\bar{c}$	19.5	20.0
I_X, slug-ft^2	4,288	3,823
I_Y, slug-ft^2	73,384	75,313
I_Z, slug-ft^2	74,867	76,738
Maximum control deflections:		
δ_r, deg	±7.5	±7.5
δ_a, deg	±7.5	±7.5

TABLE II.- LIST OF AERODYNAMIC DATA

Coefficient	Reynolds number	Basic configuration with -	Figure
C_m, $-C_X$, $-C_Z$ against α	Low	Lower rudder off; c.g. = 19.5 percent $\bar{c}$; $\delta_h = -30^\circ$	3
C_{n_β}, C_{l_β}, C_{Y_β} against α	Low	Lower rudder off	4
$\Delta C_{l,a}$, $\Delta C_{n,a}$, $\Delta C_{Y,a}$ against α	Low	Lower rudder on and off; $\delta_a = \pm 7\frac{1}{2}^\circ$	5
$\Delta C_{l,r}$, $\Delta C_{n,r}$, $\Delta C_{Y,r}$ against α	Low	Lower rudder on and off; $\delta_r = \pm 7\frac{1}{2}^\circ$	6
C_{l_p} and C_{n_r} against α	Low	Lower rudder off	7
C_m, $-C_X$, $-C_Z$ against α	High	Lower rudder on; c.g. = 20 percent $\bar{c}$; $\delta_h = -35^\circ$	8
C_{n_β}, C_{l_β}, C_{Y_β} against α	High	Lower rudder on	9
C_{n_β} and C_{l_β} against α	High	Lower rudder off	10
C_m[1] against α	-------	----------	11
C_{m_q} against α	335,000	Lower rudder off; $\delta_h = -35^\circ$	12

[1]Arbitrary values of C_m used.

TABLE III.- INITIAL CONDITIONS USED IN CALCULATIONS

	Column A	Column B	Column C	Column D
α, deg	15	20	80	15
β, deg	-15	-15	-1	-15
θ_e, deg	-60	20	-10	-60
ϕ, deg	-5	-9	0	-5
δ_r, deg	0	0	7.5	0
δ_a, deg	0	0	-7.5	0
u, ft/sec	246	240	443	246
v, ft/sec	-68	-68	-4	-68
w, ft/sec	66	87	251	66
p, radians/sec	0	0	.243	0
q, radians/sec	.7	.3	0	.7
r, radians/sec	0	0	1.379	0
h_1, ft	19,000	19,000	30,000	30,000

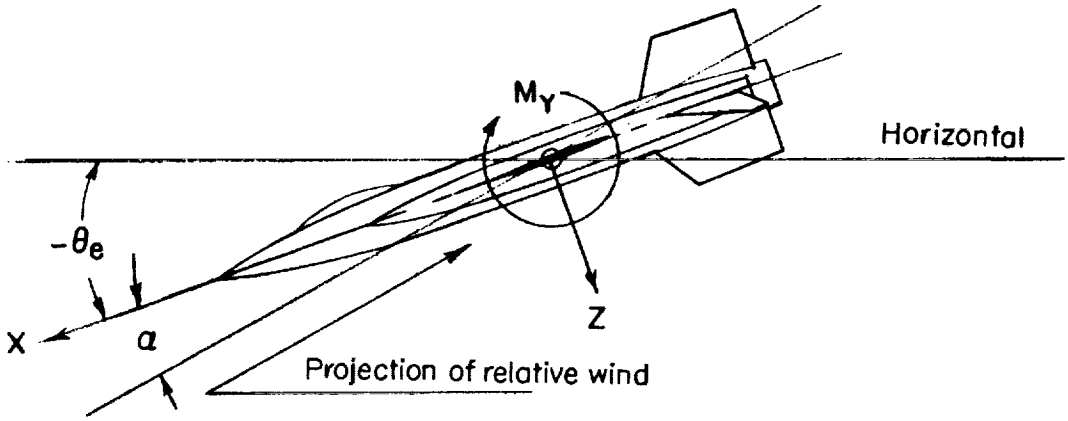

(a) ϕ_e and $\psi_e = 0$.

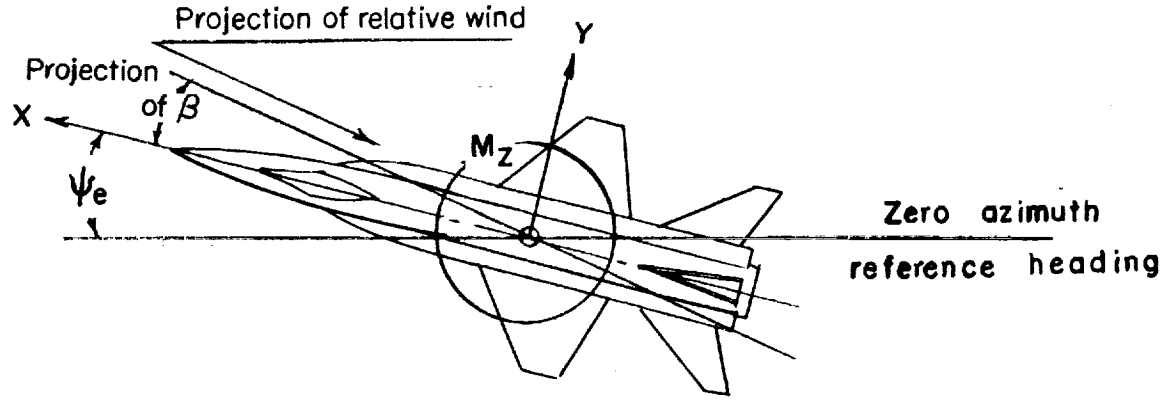

(b) θ_e and $\phi_e = 0$.

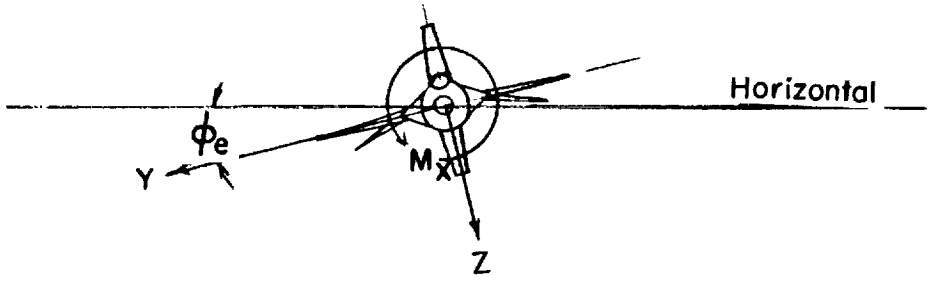

(c) θ_e and $\psi_e = 0$, and in this case $\phi = \phi_e$.

Figure 1.- Body system of axes and related angles.

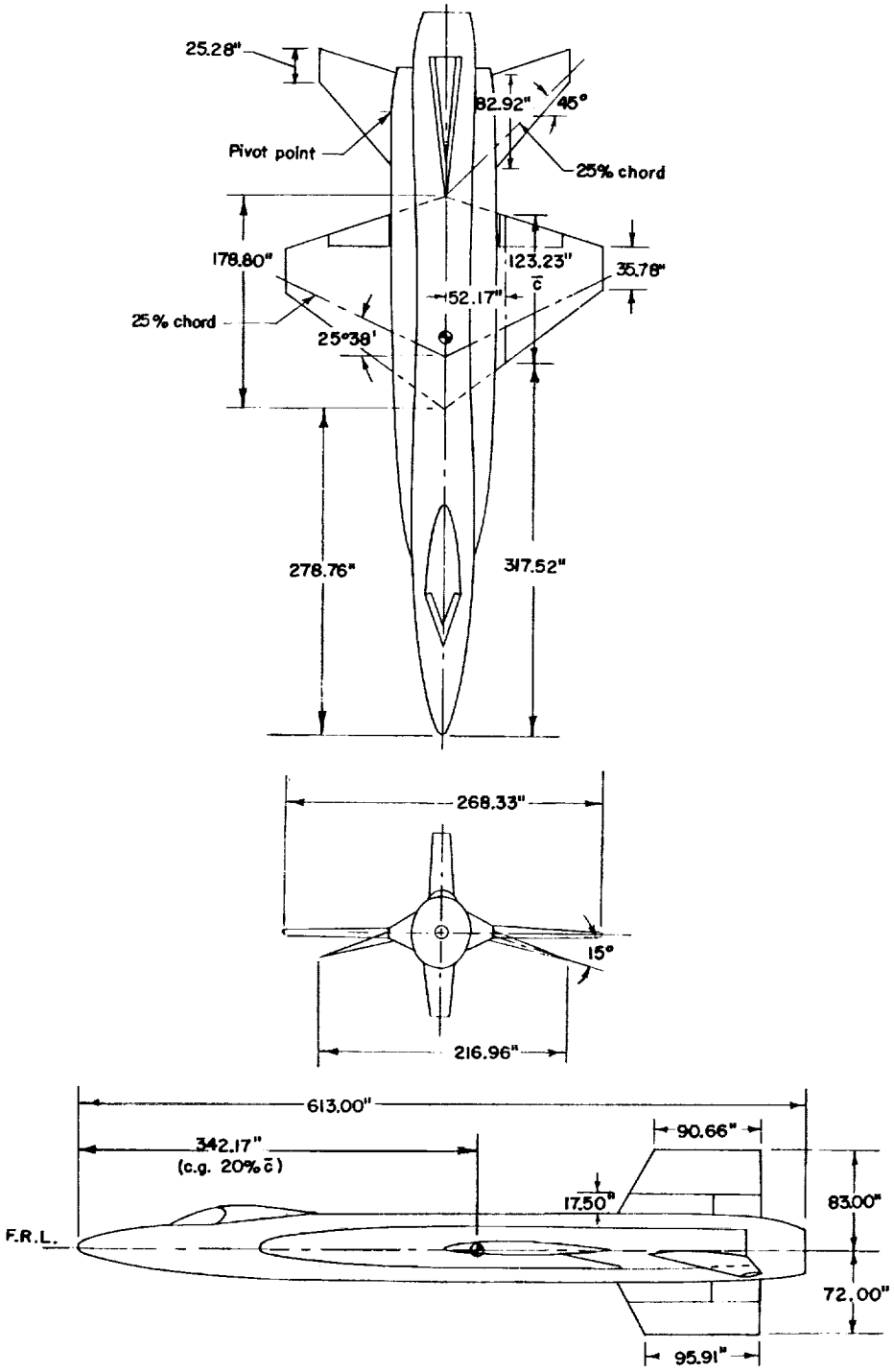

Figure 2.- Three-view drawing of the North American X-15 airplane. (Dimensions are full scale.)

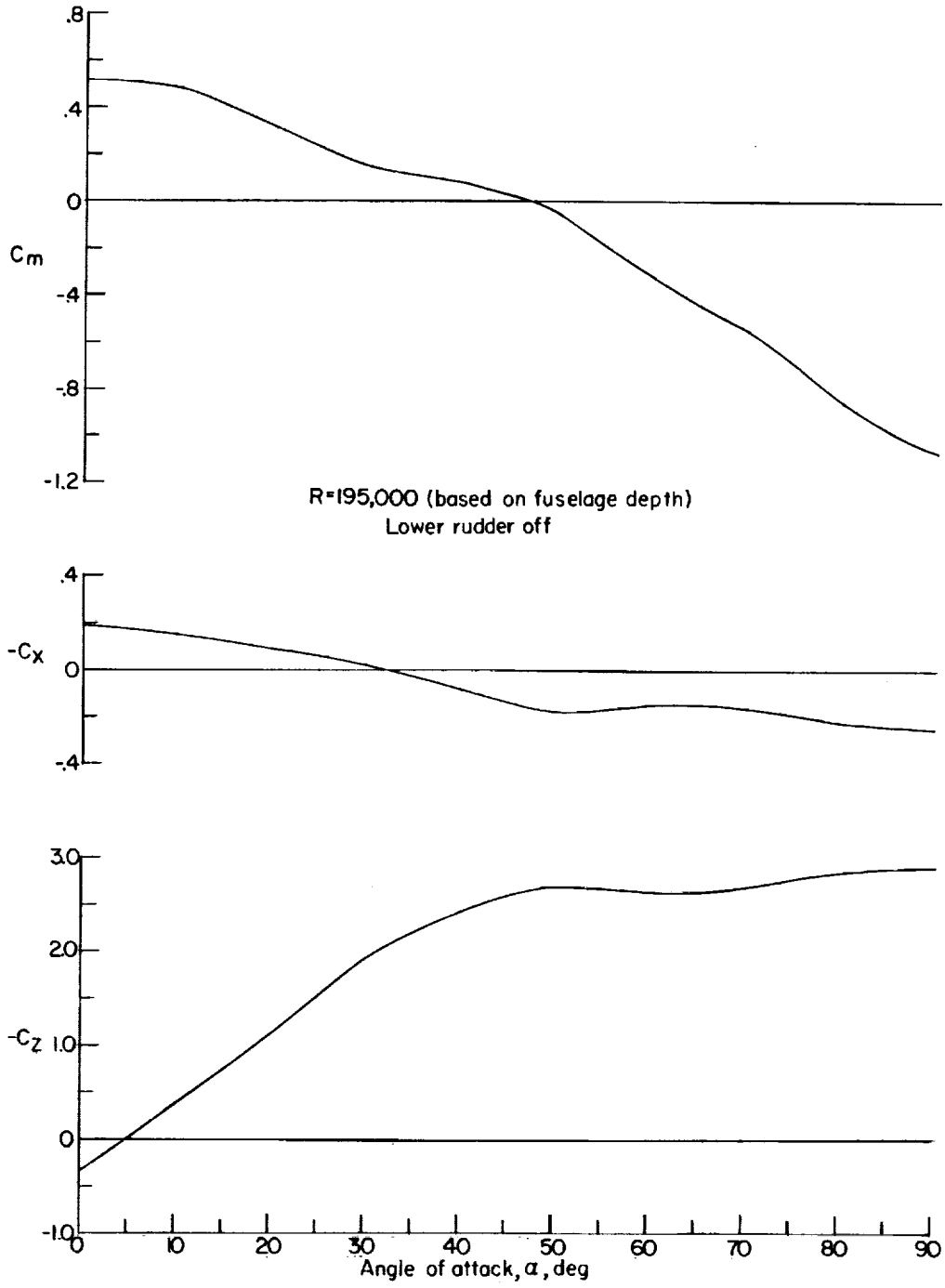

Figure 3.- Variations of pitching-moment, axial-force, and normal-force coefficients with angle of attack. Center of gravity, 19.5 percent $\bar{c}$; $\delta_h = -30^\circ$.

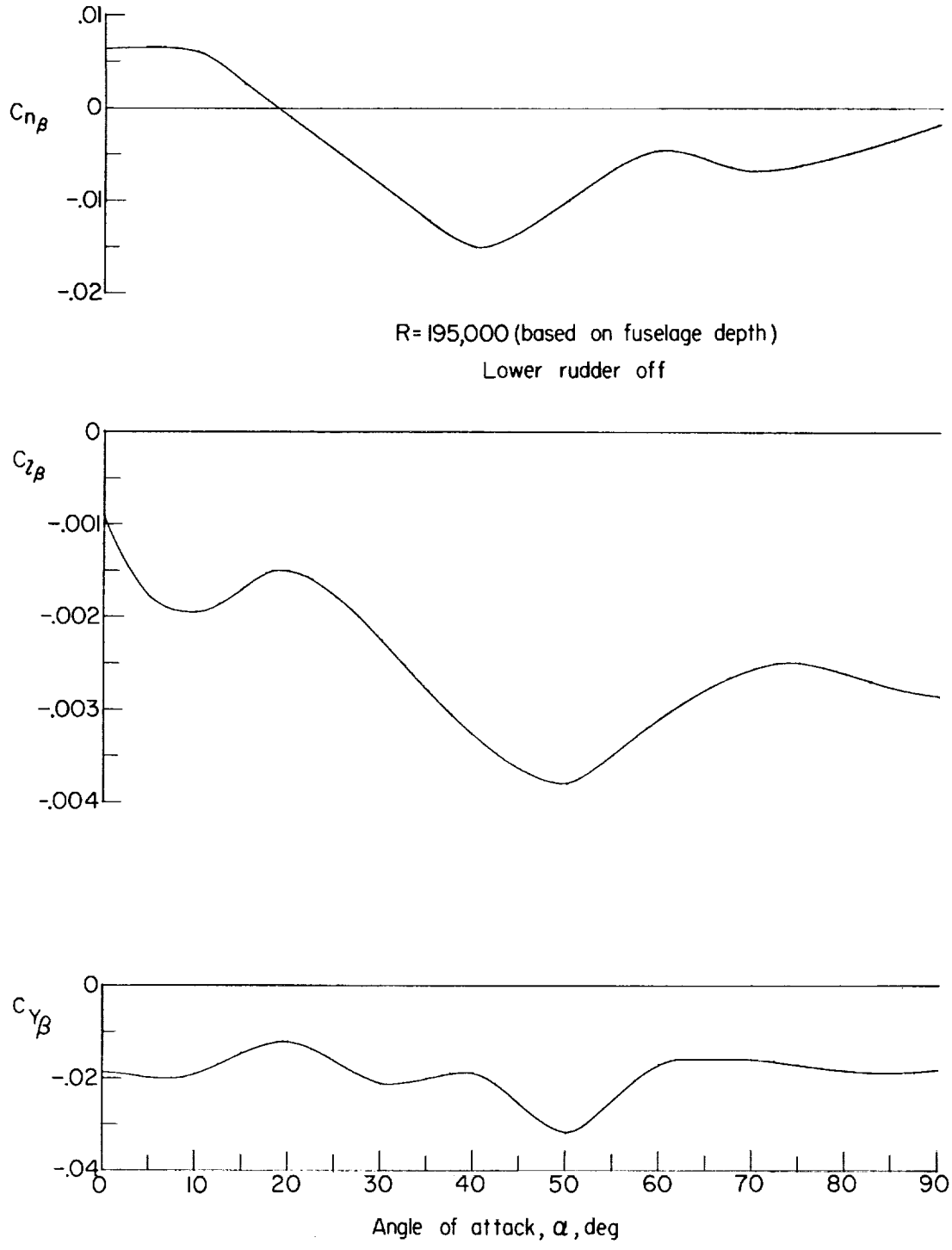

Figure 4.- Variation of sideslip derivatives with angle of attack.

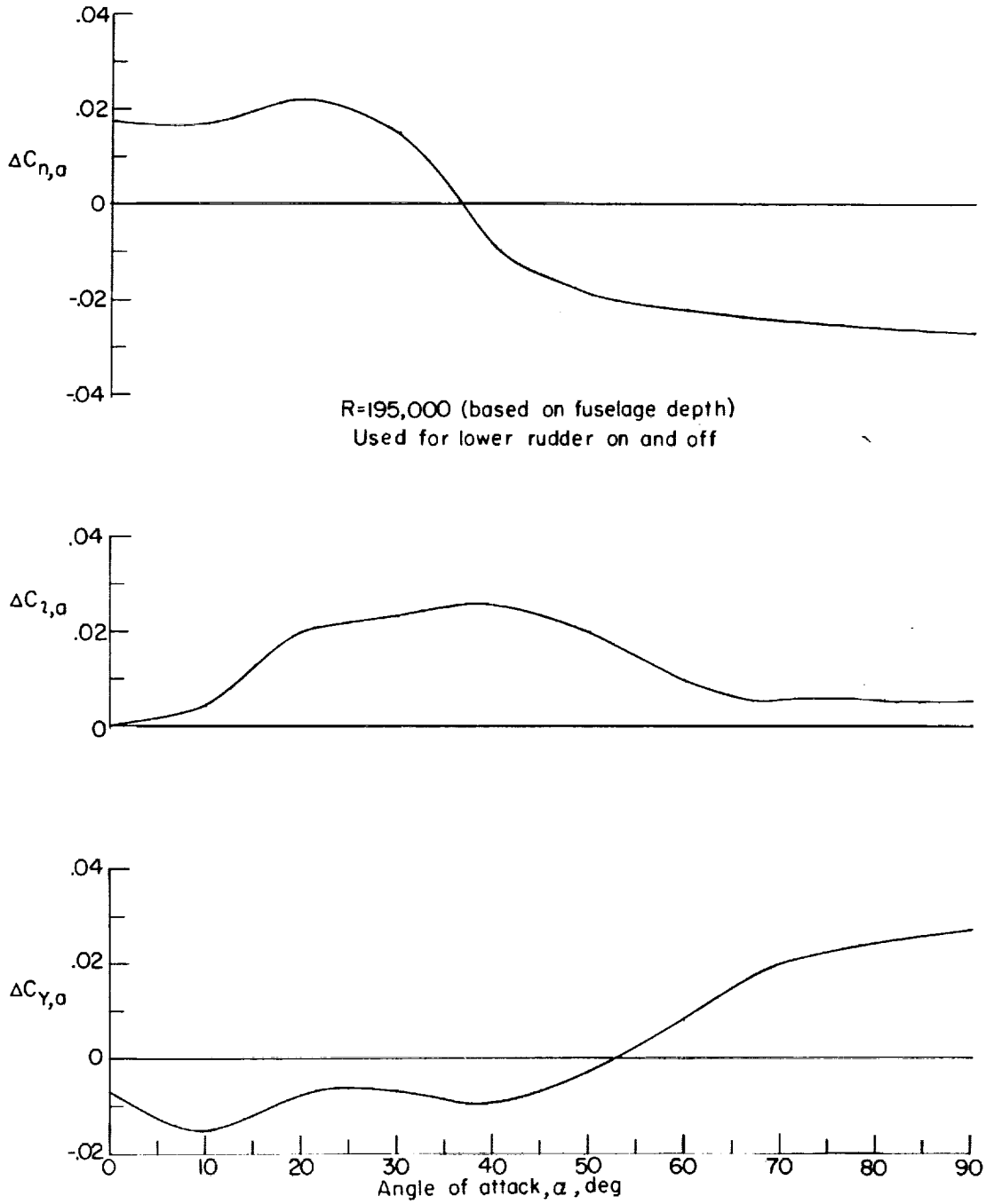

Figure 5.- Variation in increments in the lateral force and moment coefficients with angle of attack due to aileron deflection. $\delta_a = \pm 7\frac{1}{2}^{\circ}$.

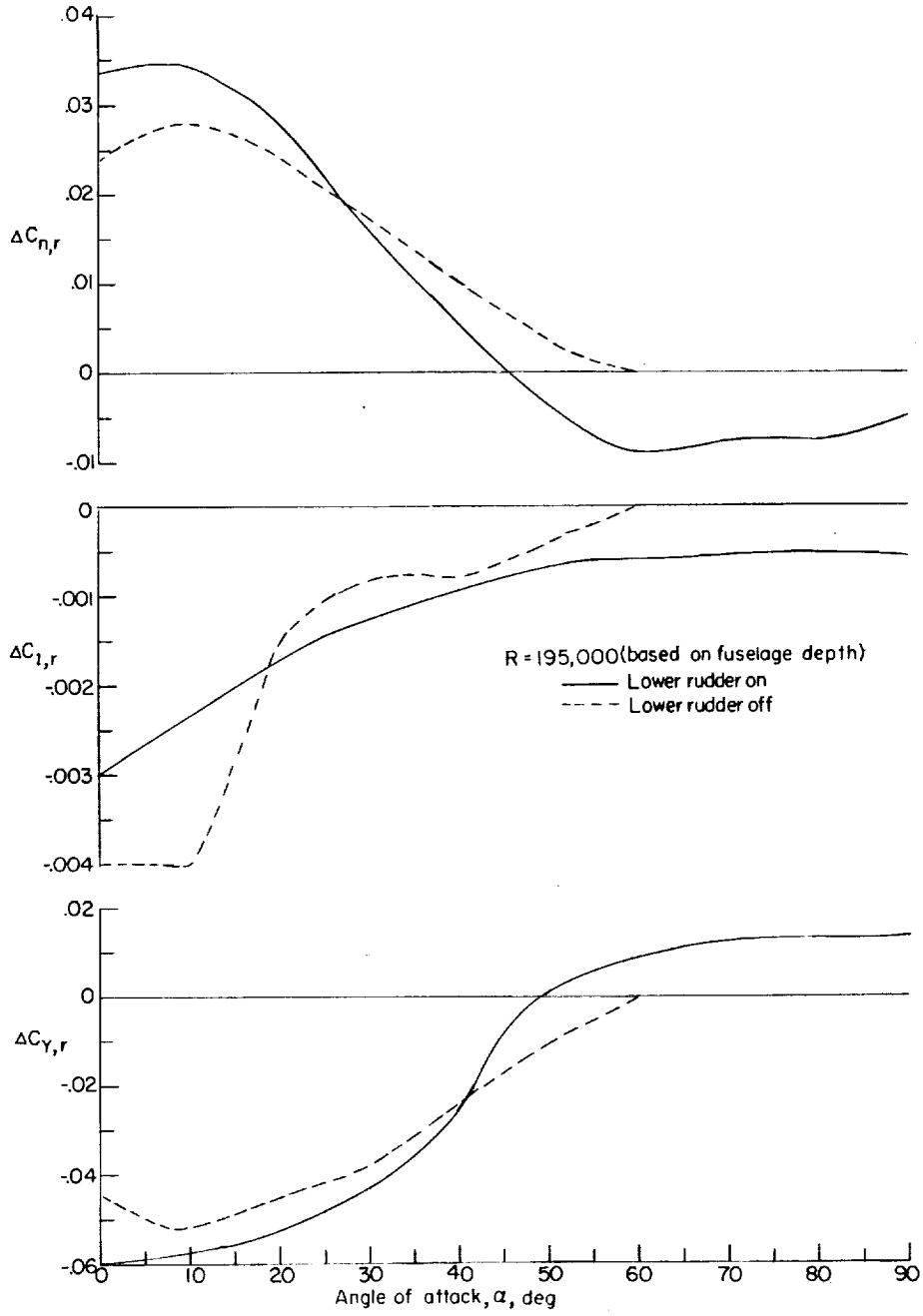

Figure 6.- Variation in increments in the lateral force and moment coefficients with angle of attack due to deflecting rudder. $\delta_r = \pm 7\frac{1}{2}^\circ$.

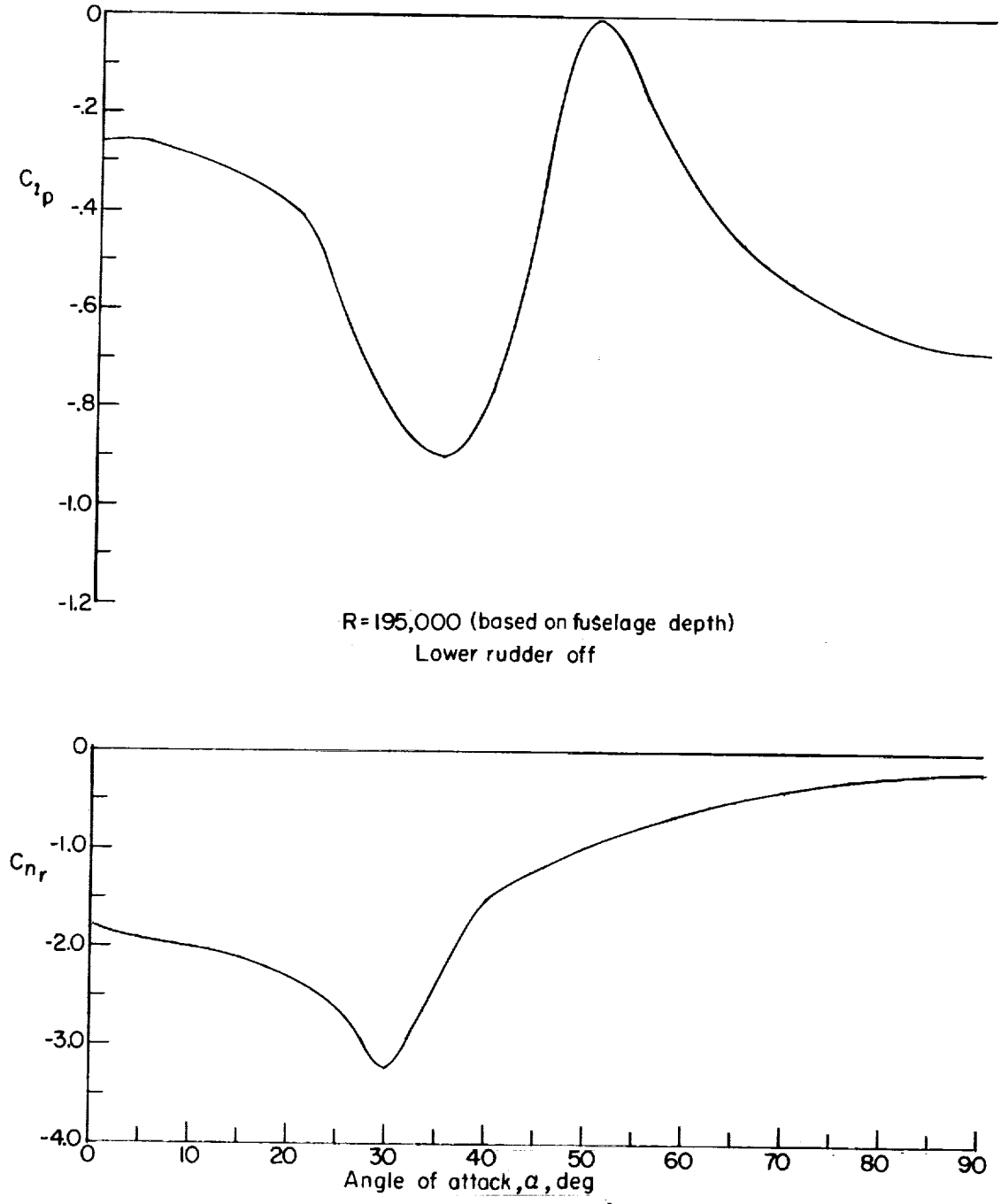

Figure 7.- Variations of the damping-in-roll and damping-in-yaw derivatives with angle of attack.

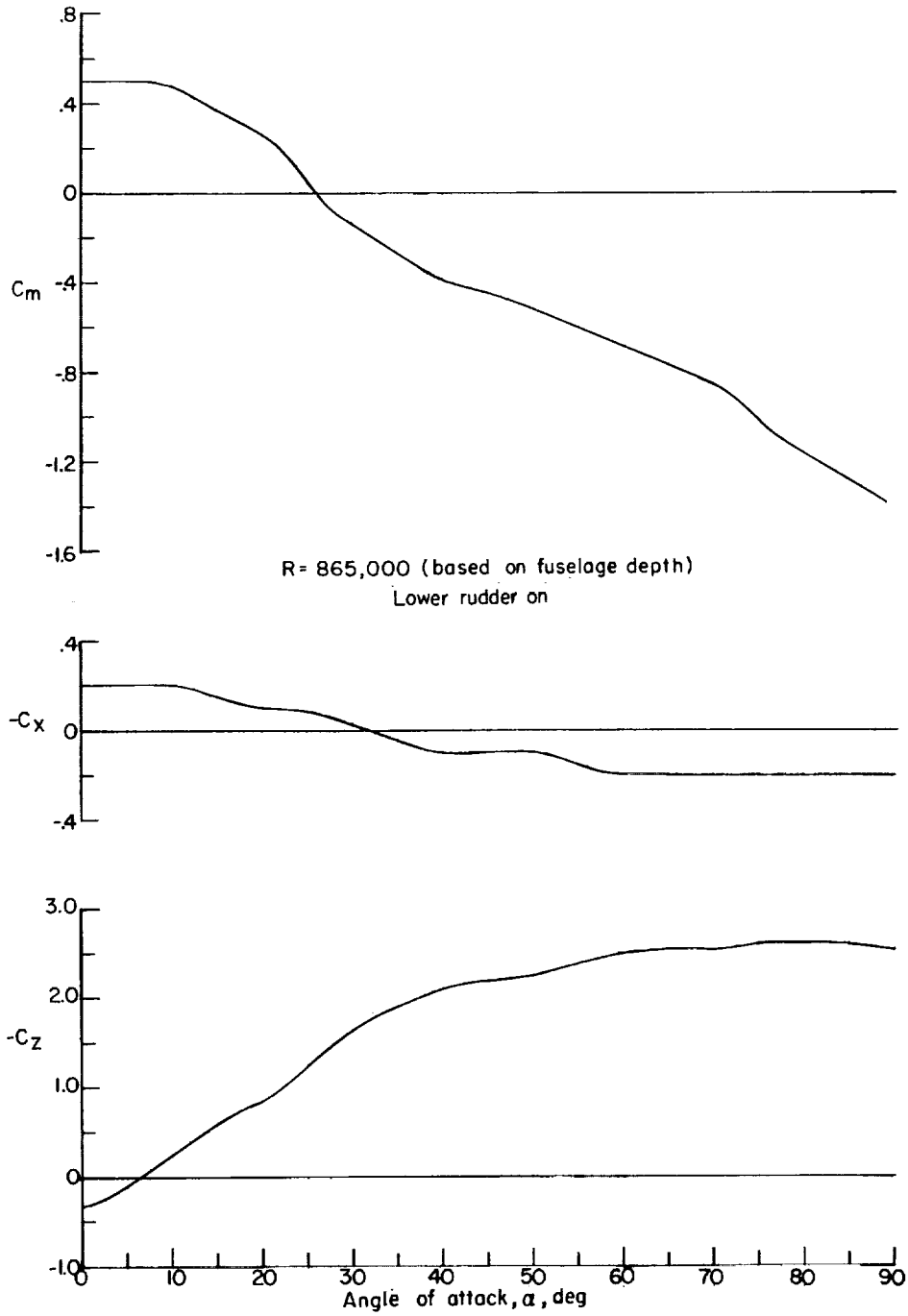

Figure 8.- Variations of pitching-moment, axial-force, and normal-force coefficients with angle of attack. Center of gravity, 20 percent $\bar{c}$; $\delta_h = -35^\circ$.

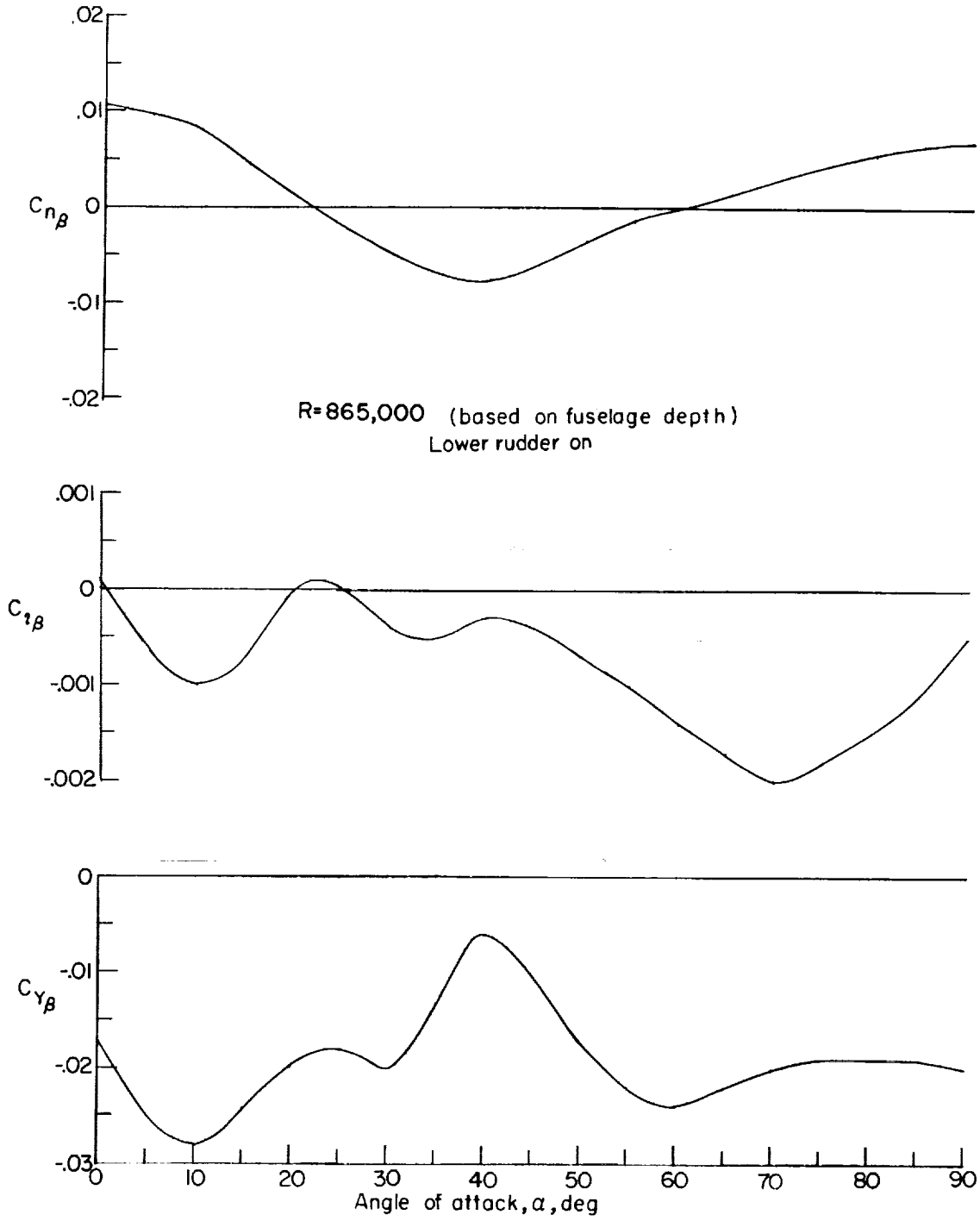

Figure 9.- Variation of sideslip derivatives with angle of attack.

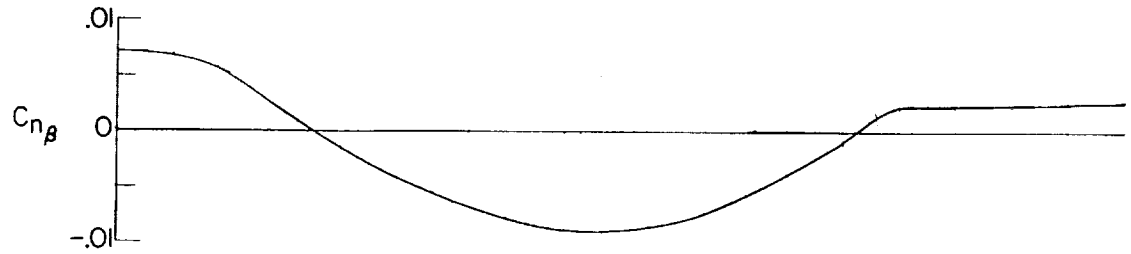

R=865,000 (based on fuselage depth)
Lower rudder off

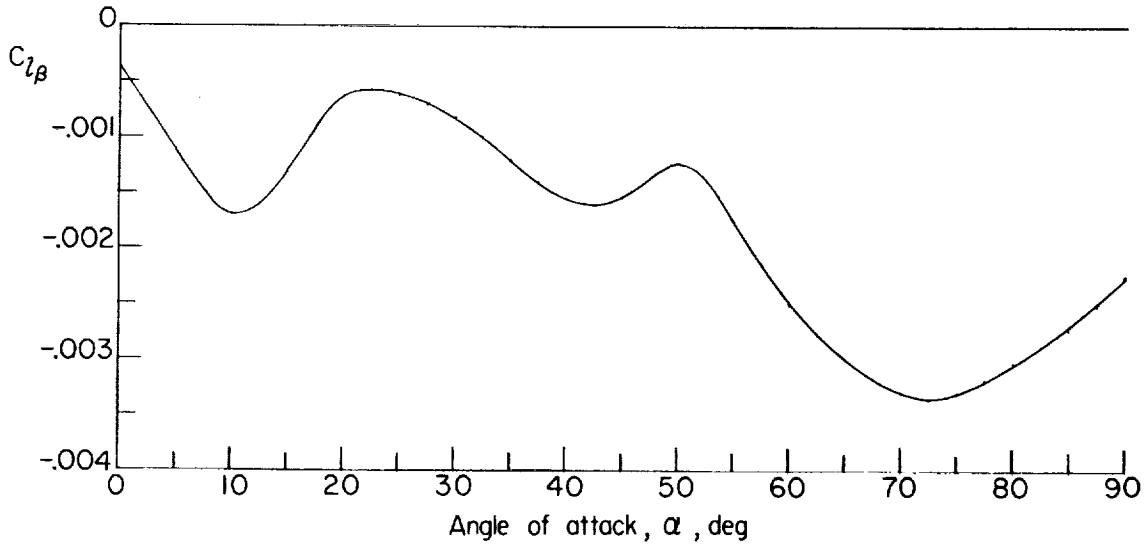

Figure 10.- Variation of yawing and rolling sideslip derivatives with angle of attack.

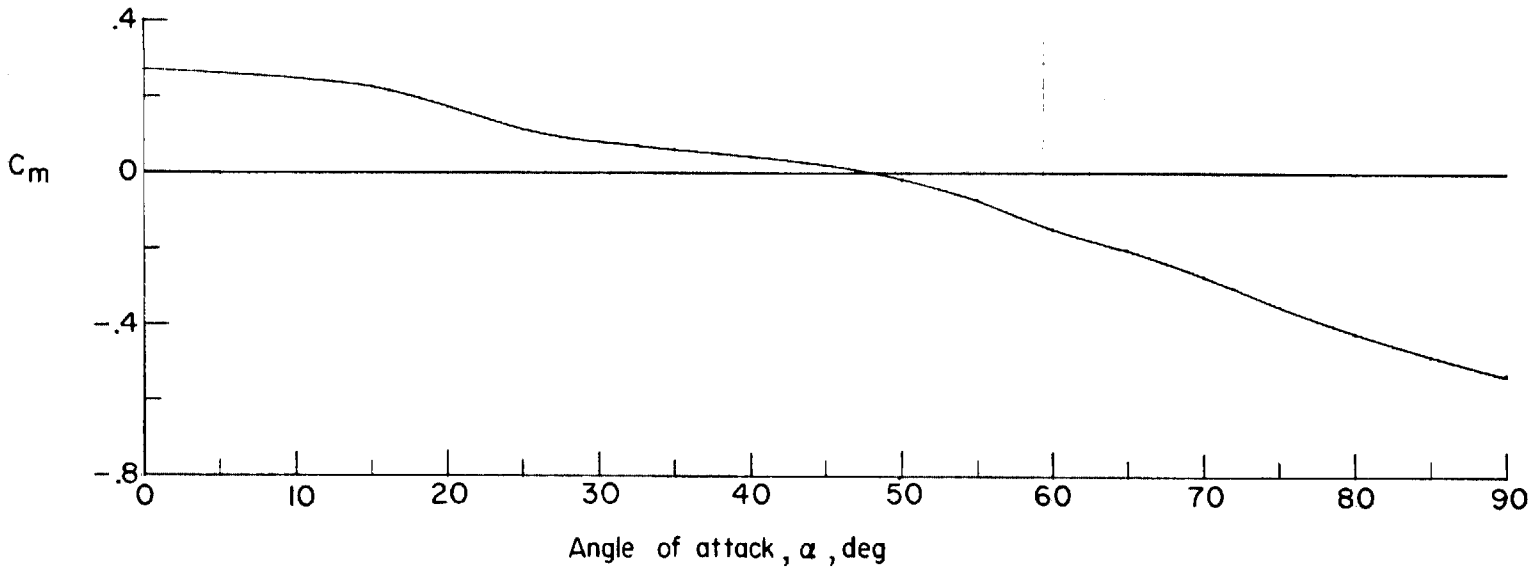

Figure 11.- Variation of pitching-moment coefficient with angle of attack. (Arbitrary values of C_m.)

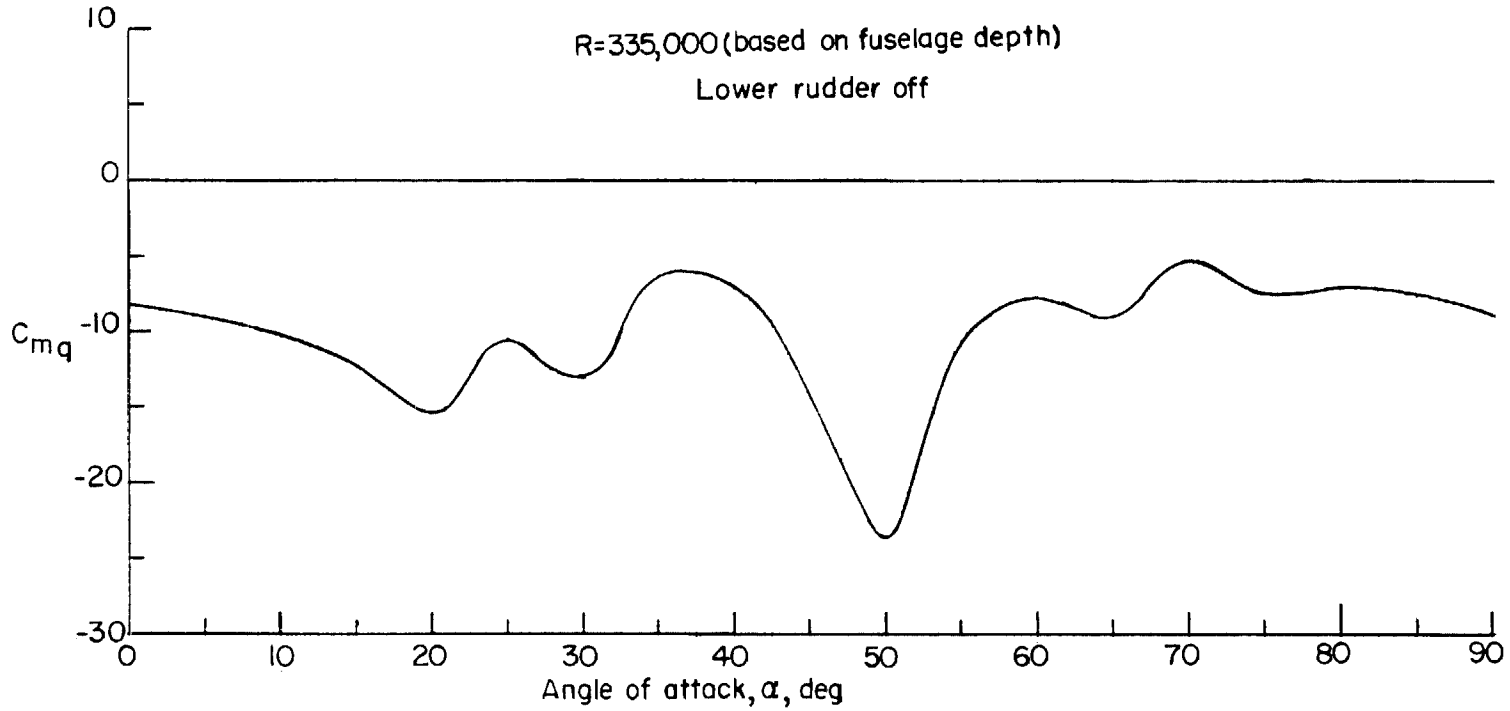

Figure 12.- Variation of the damping-in-pitch derivative with angle of attack.

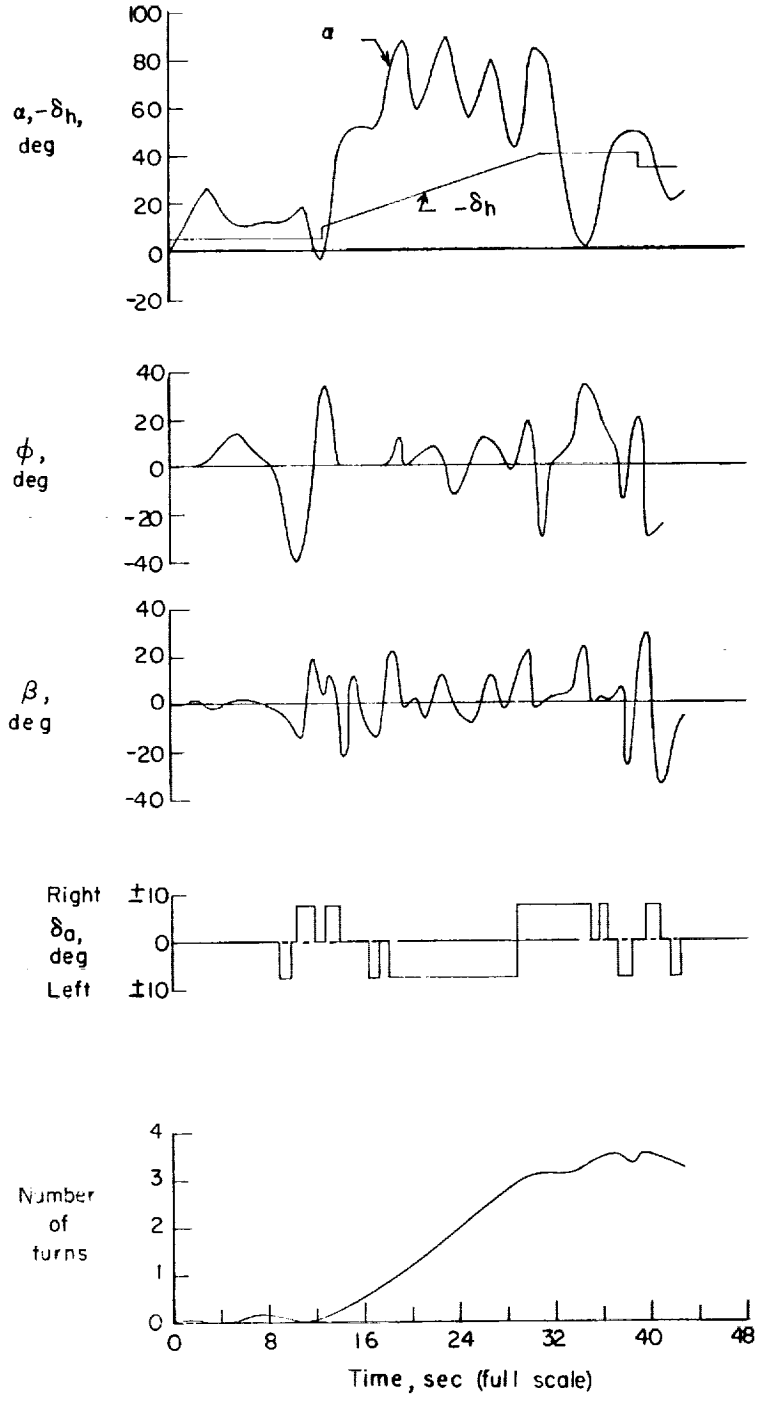

Figure 13.- Results of radio-controlled dynamic-model test for lower-rudder-off configuration. (Data from ref. 5.)

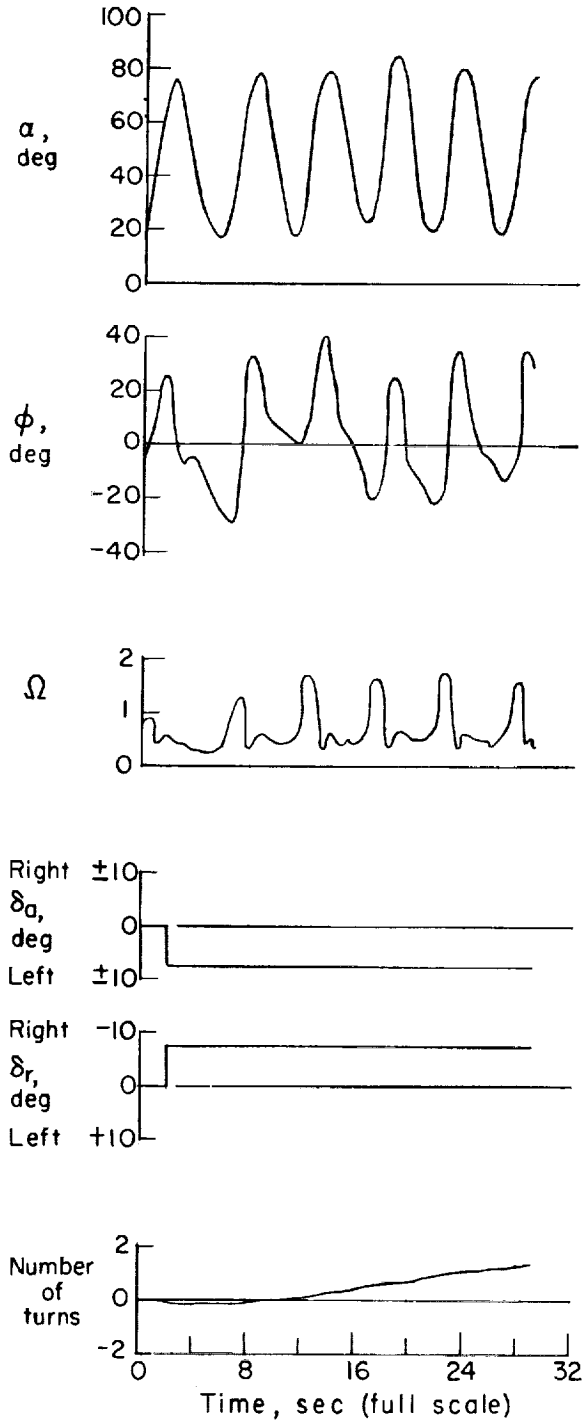

Figure 14.- Results of initial calculated spin-entry attempt. Low Reynolds number; lower rudder off.

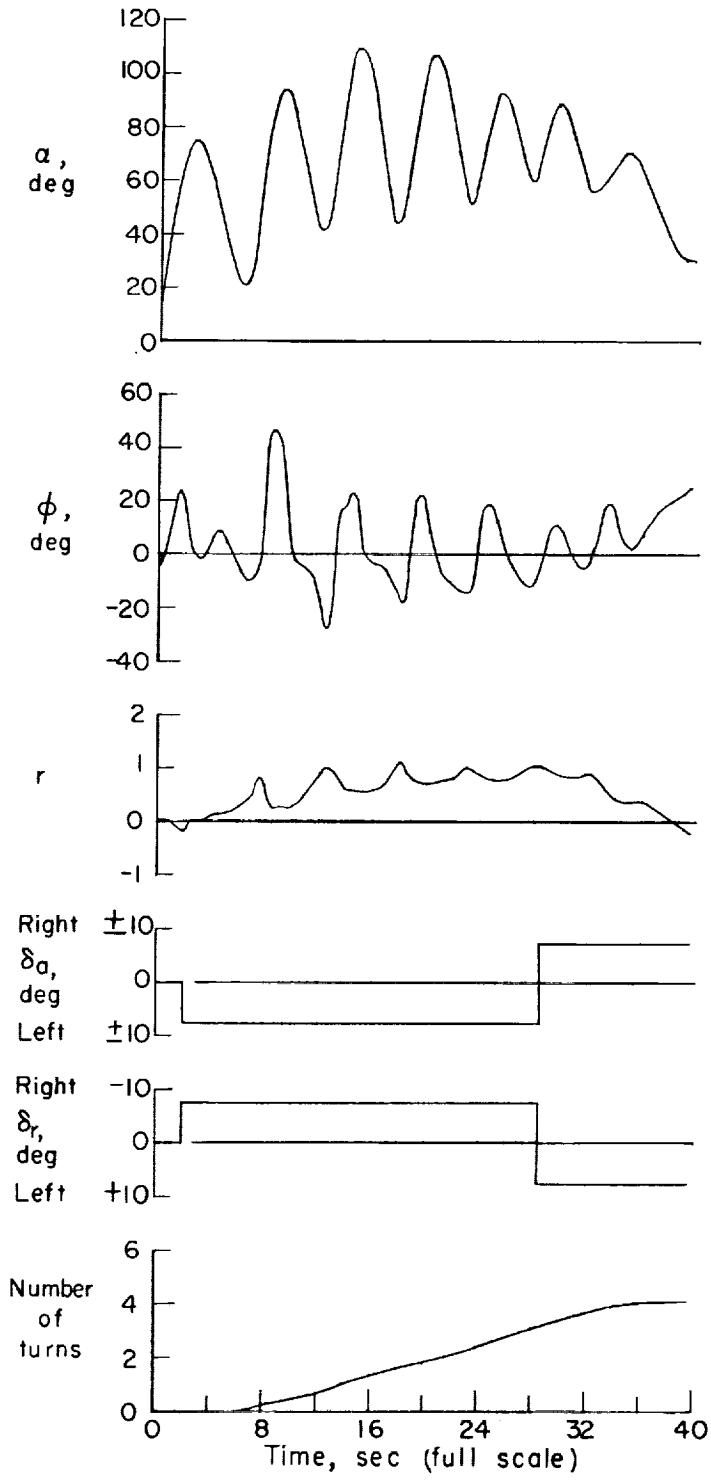

Figure 15.- Spin entry, spin, and recovery calculated for low Reynolds number. Lower rudder off; C_m approximately 50 percent of measured static values.

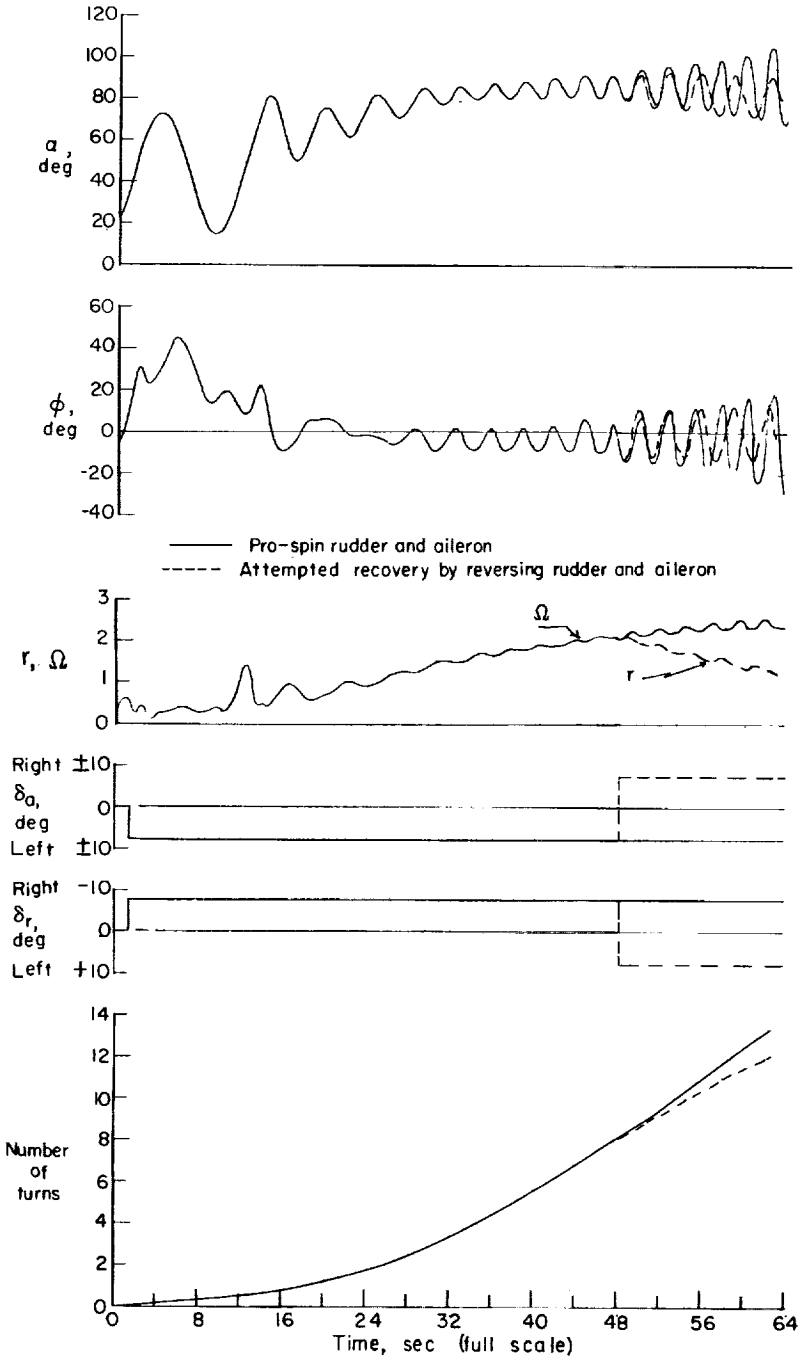

Figure 16.- Spin entry, spin, and recovery calculated from a nose-up initial attitude for low Reynolds number. Lower rudder off; C_m approximately 50 percent of measured static values.

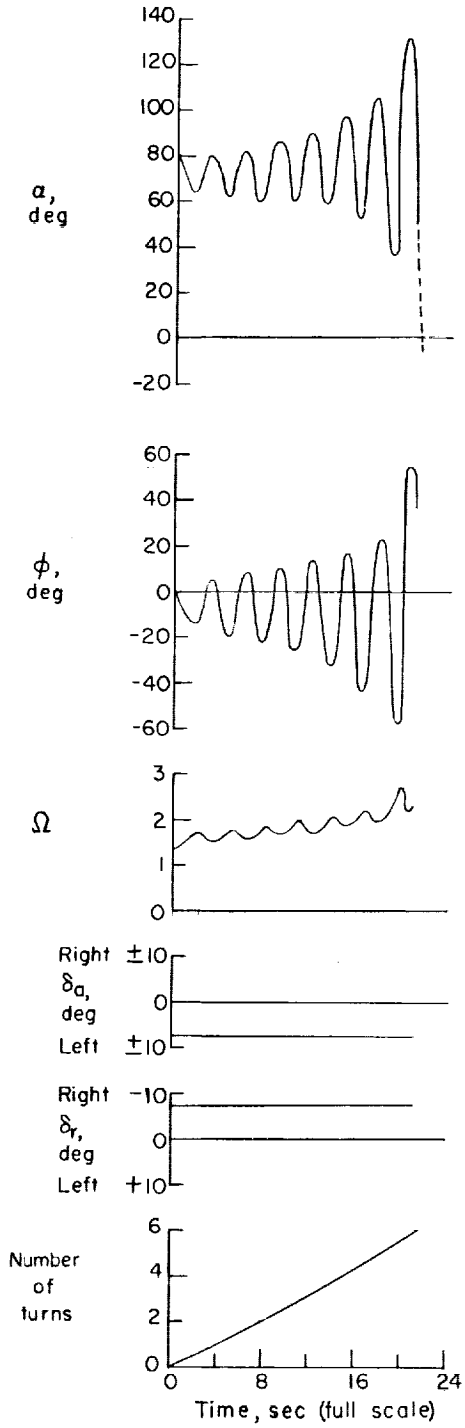

Figure 17.- Calculation simulating spin-tunnel model prerotated launching technique at high Reynolds number. Lower rudder on.

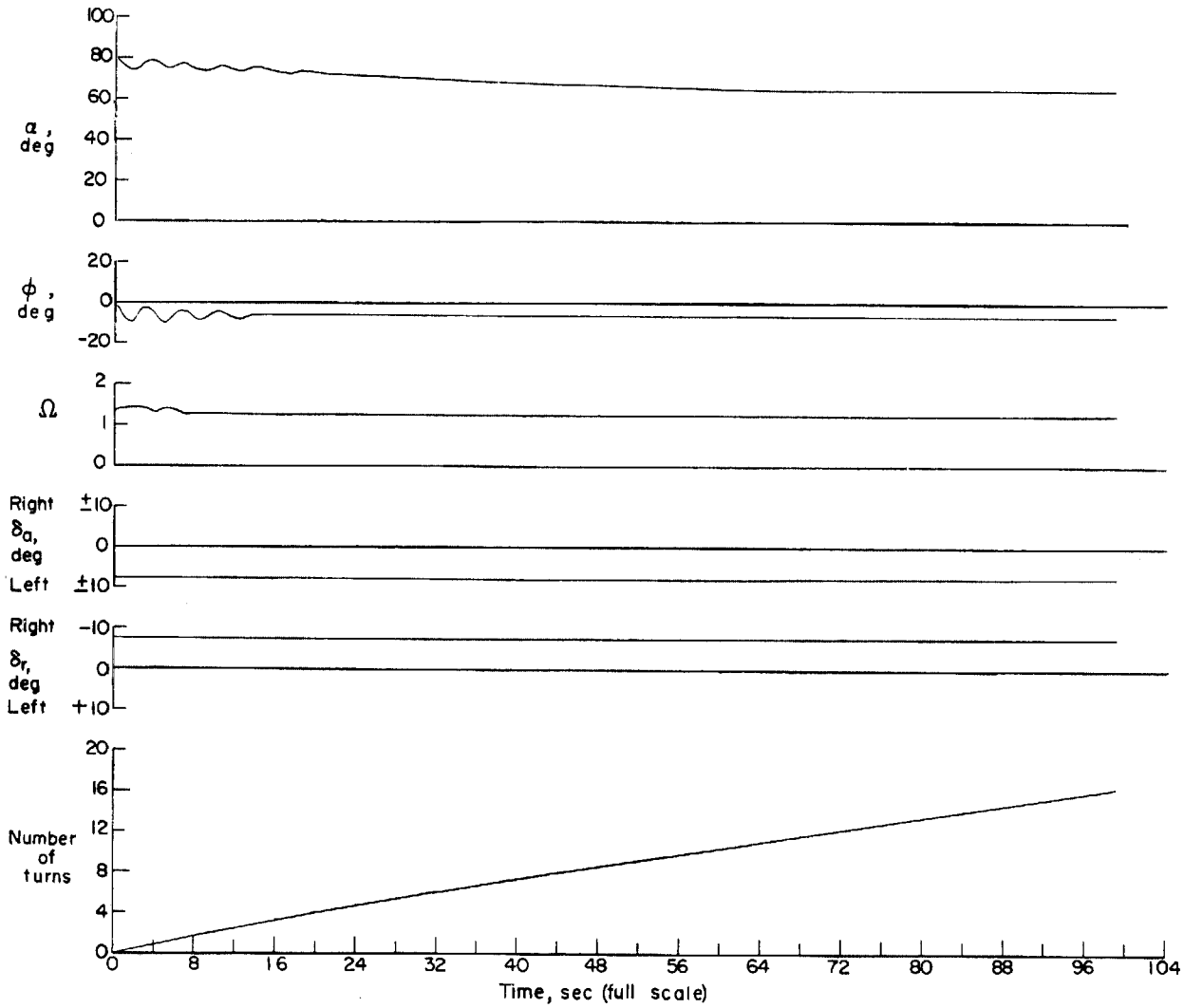

Figure 18.- Calculation simulating spin-tunnel model prerotated launching technique at high Reynolds number. Lower rudder on; C_m approximately 50 percent of measured static values.

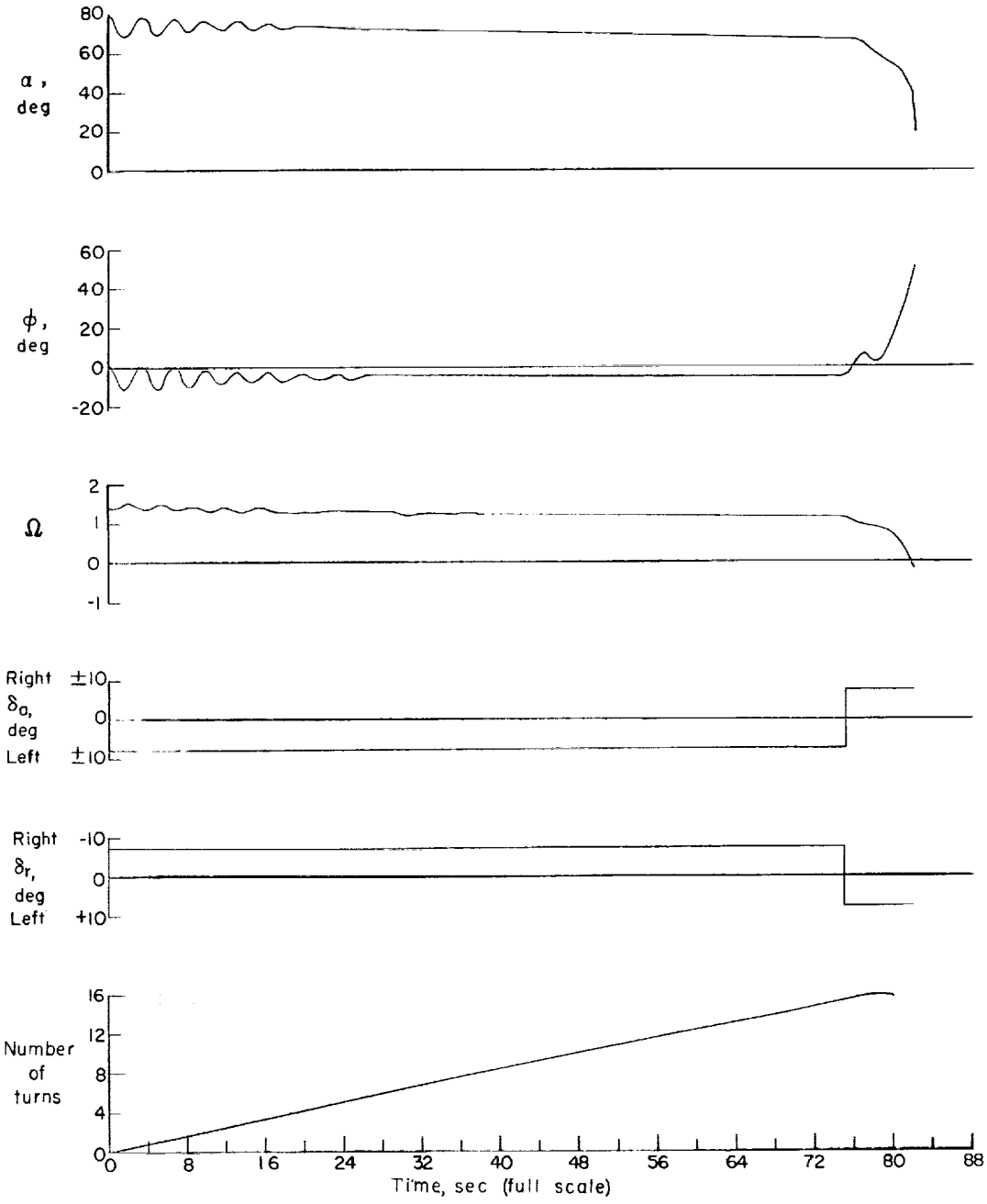

Figure 19.- Calculation simulating spin-tunnel model prerotated launching technique at high Reynolds number. Lower rudder on; C_m approximately 70 percent of measured static values.

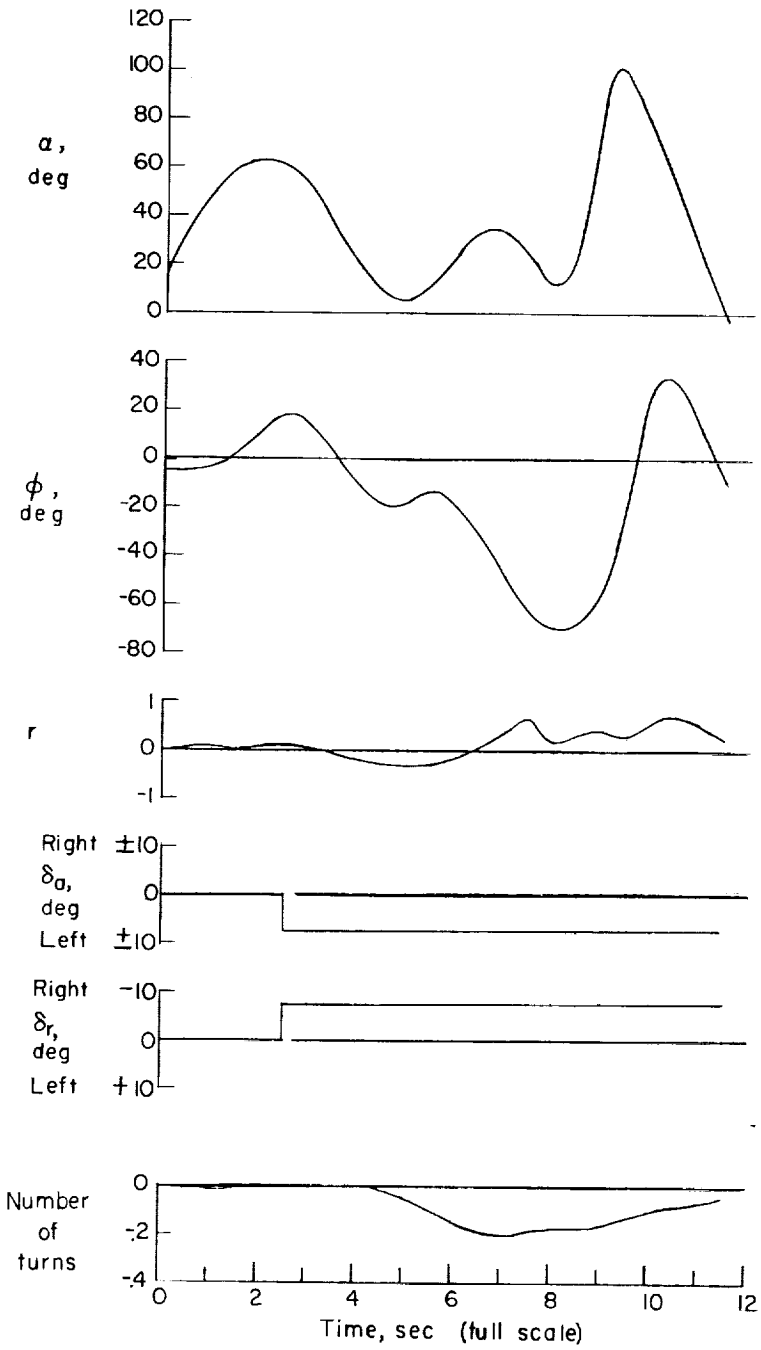

Figure 20.- Calculated spin-entry attempt at high Reynolds number. Lower rudder on; C_m approximately 70 percent of measured static values.

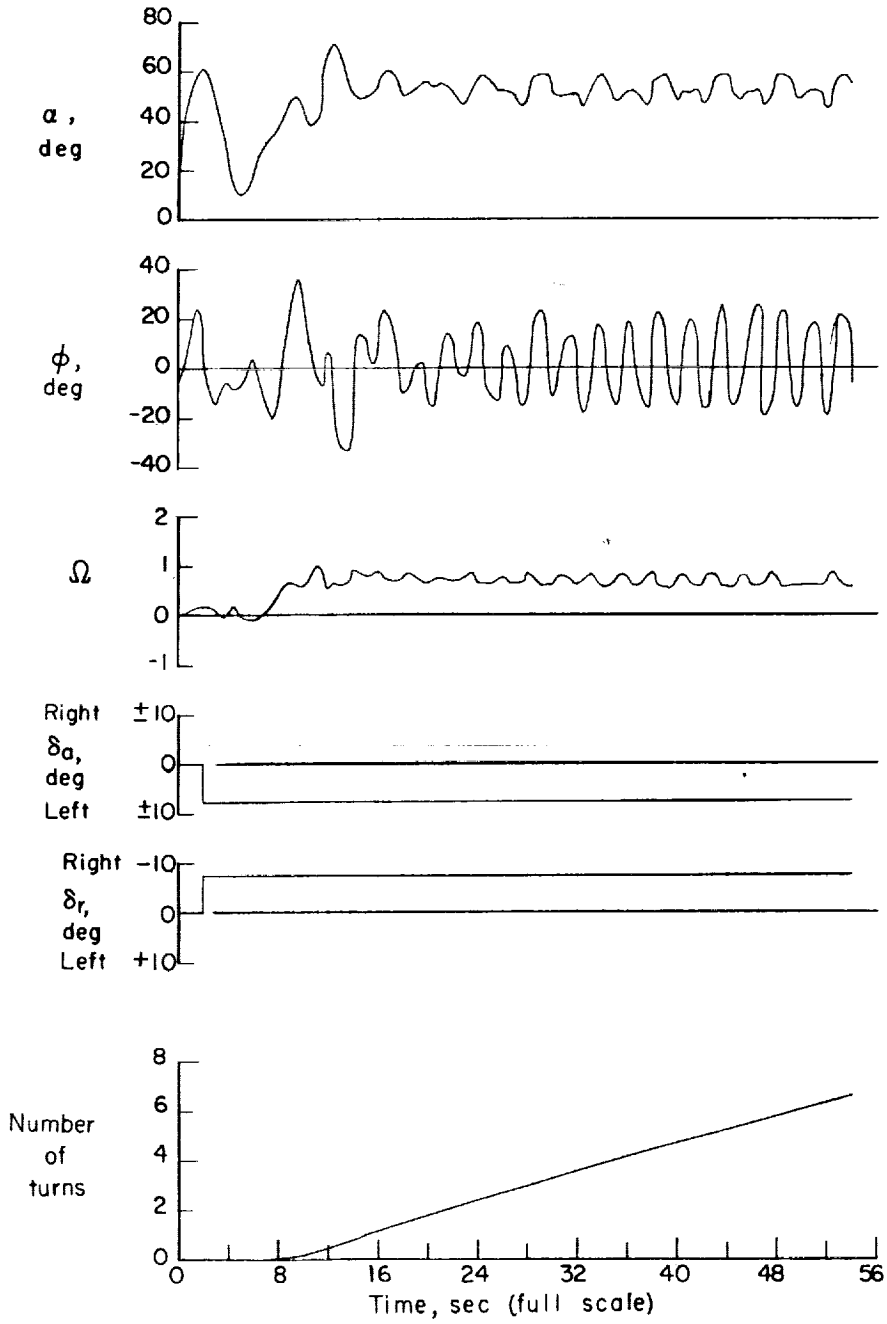

Figure 21.- Calculated spin entry and spin for high Reynolds number. Lower rudder on; C_m approximately 70 percent of measured static values; larger negative C_{l_β} values used (see fig. 4).

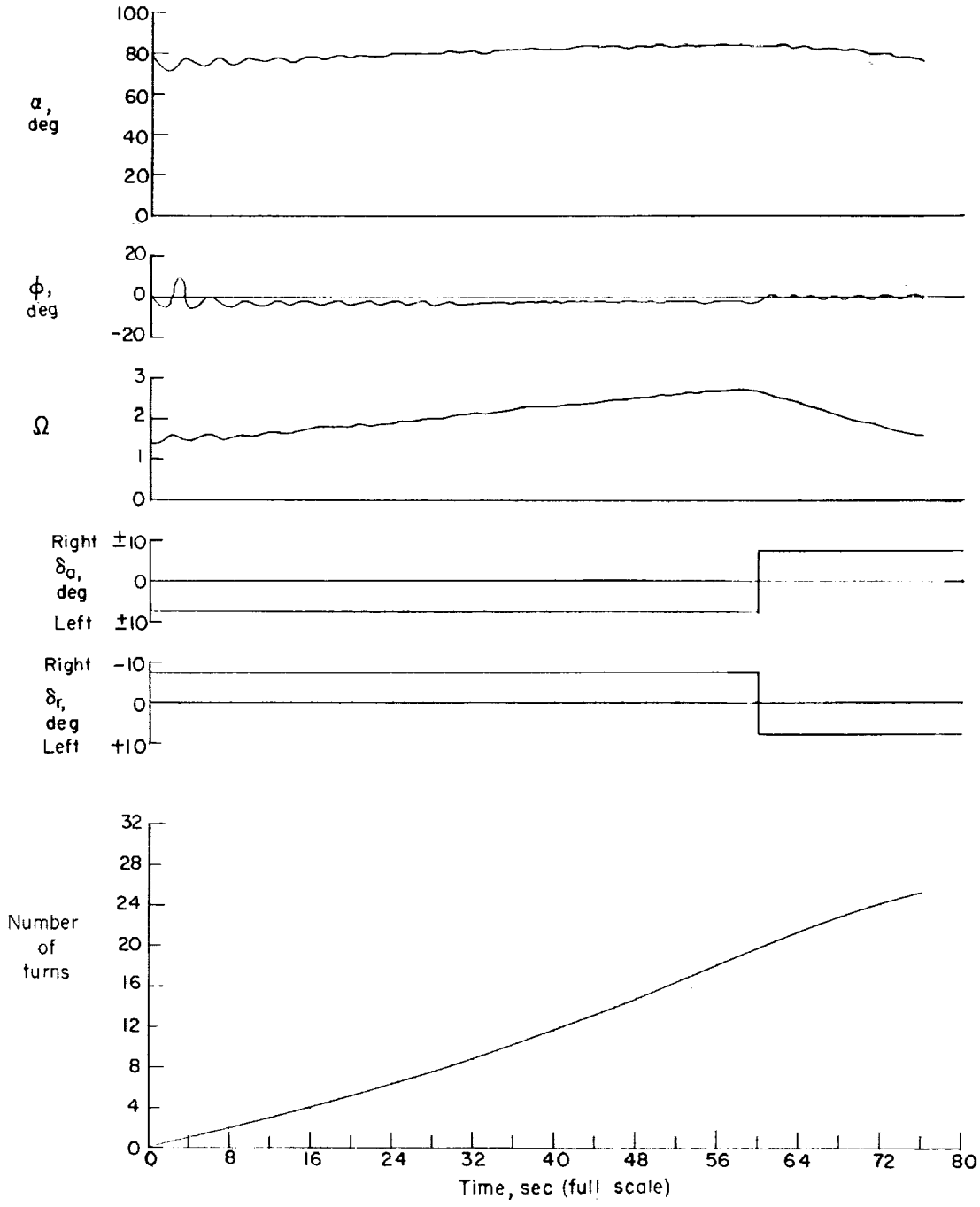

Figure 22.- Calculation simulating spin-tunnel model prerotated launching technique at high Reynolds number. Lower rudder off; C_m approximately 70 percent of measured static values.

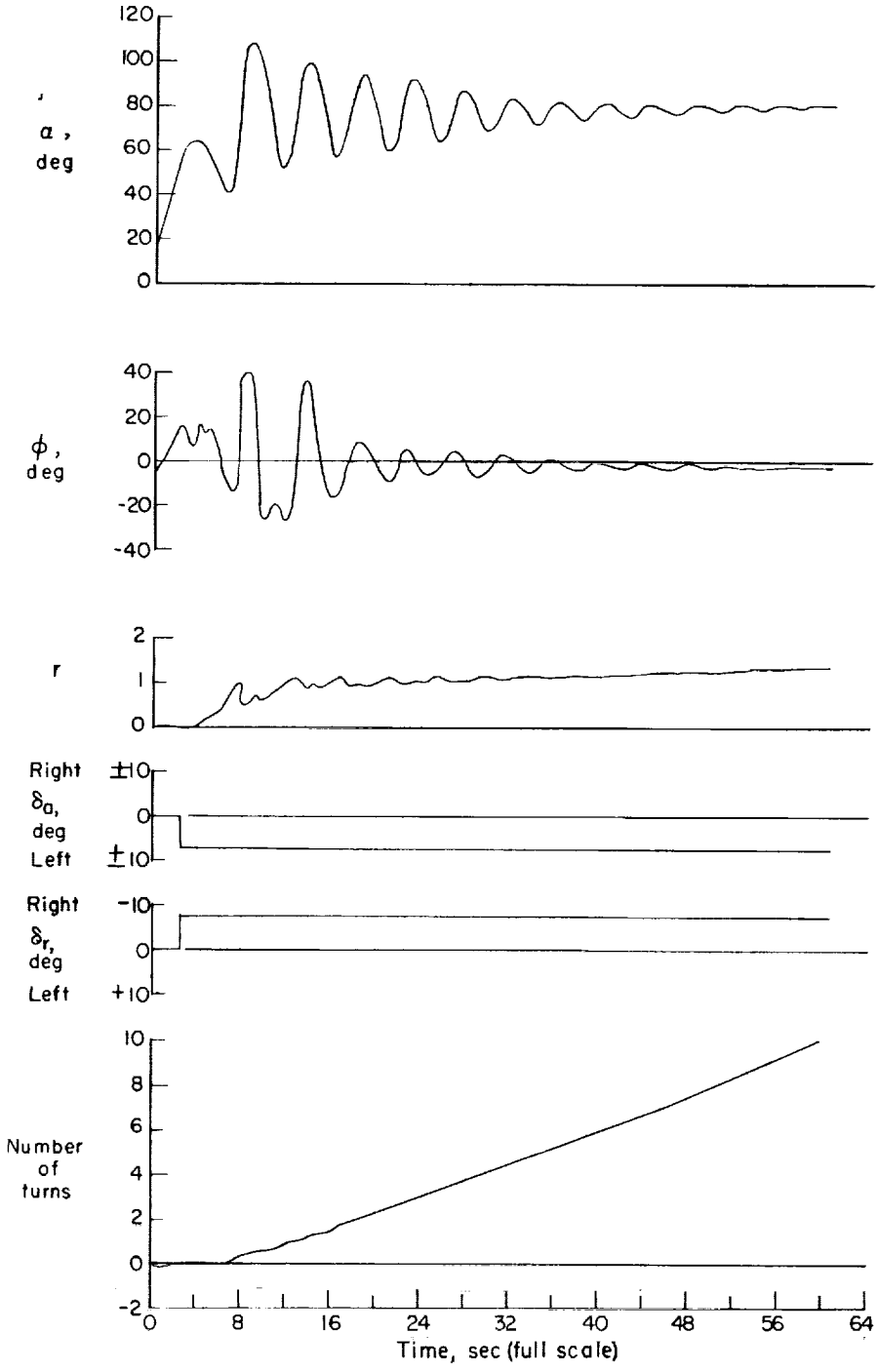

Figure 23.- Calculated spin entry and spin for high Reynolds number. Lower rudder off; arbitrarily reduced C_m values used (see fig. 11).

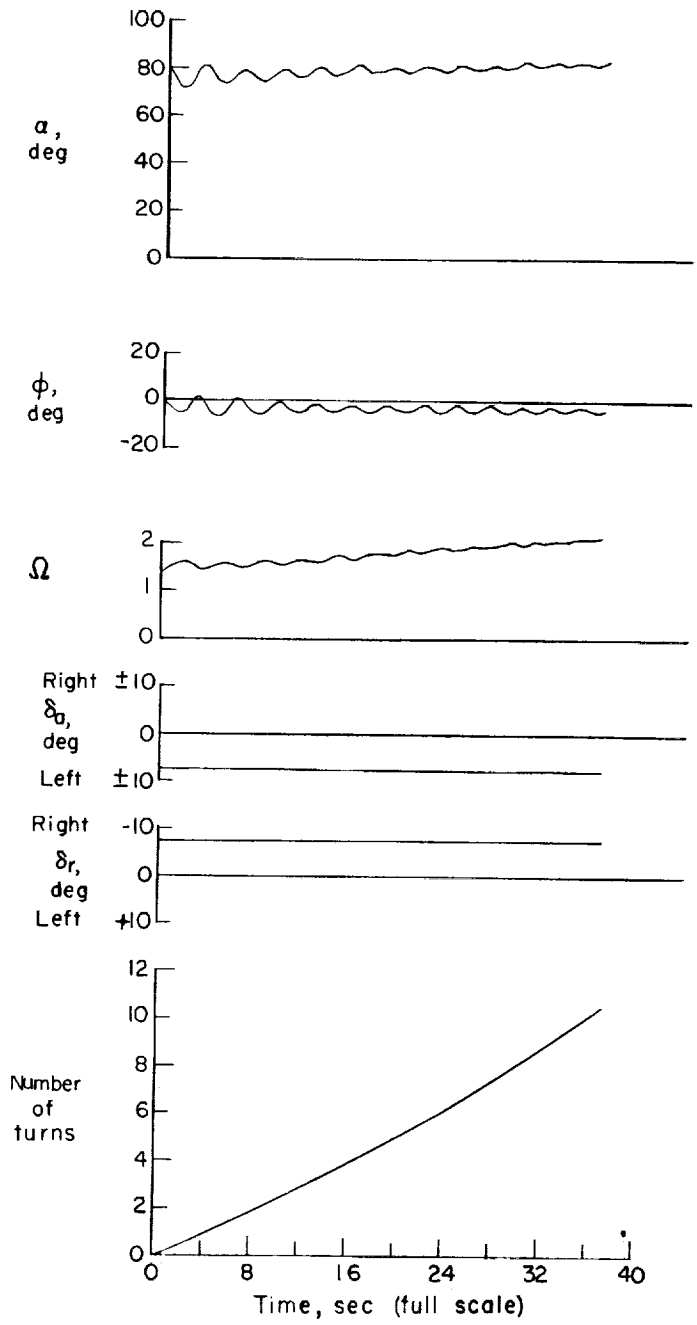

Figure 24.- Calculation simulating spin-tunnel model prerotated launching technique at high Reynolds number. Lower rudder off; C_m approximately 70 percent of measured static values; $C_{m_q} = -5.0$.

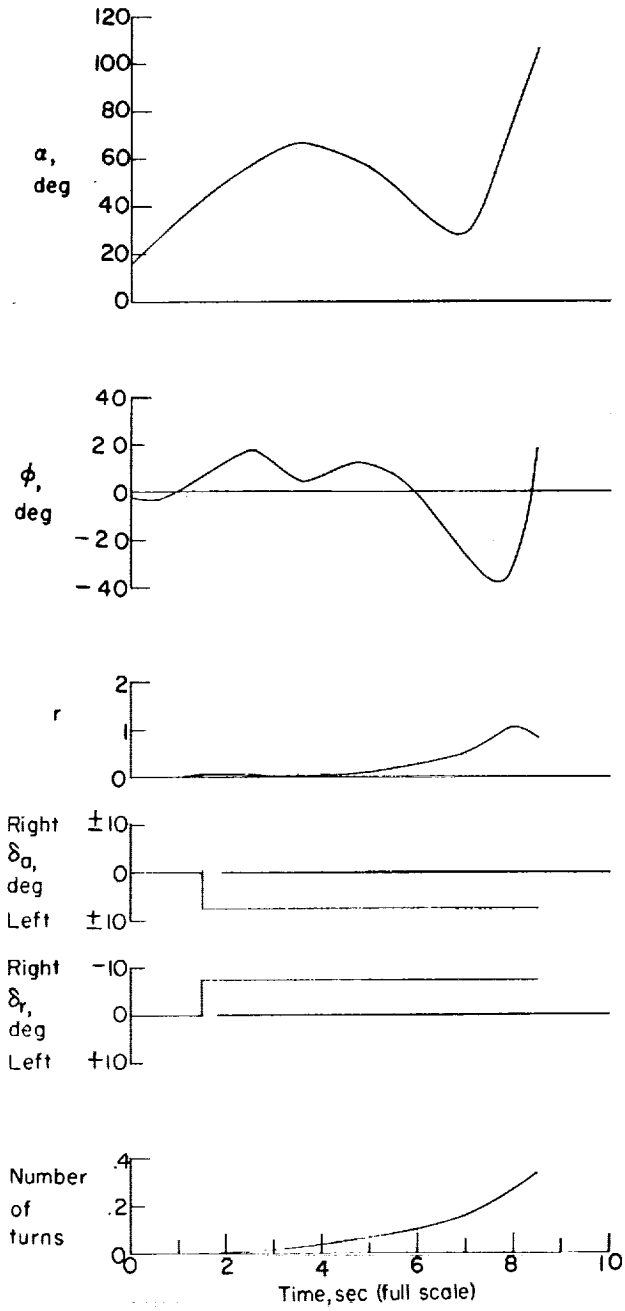

Figure 25.- Calculated spin-entry attempt at high Reynolds number. Lower rudder off; arbitrarily reduced C_m values used (see fig. 11); $C_{m_q} = -7.0$.

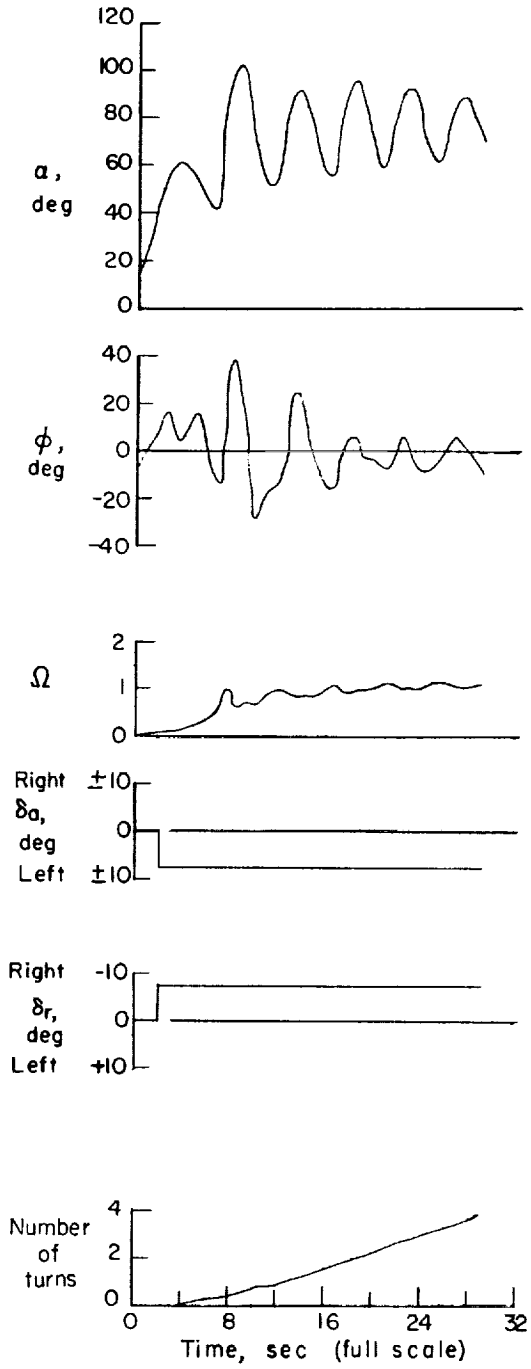

Figure 26.- Calculated spin entry and spin for high Reynolds number. Lower rudder off; arbitrarily reduced C_m values used (see fig. 11); curve of C_{m_q} against α in figure 12 used.